CORRELATION OF SEISMIC REFLECTION DATA WITH SEISMICITY OVER THE RAMAPO, NEW JERSEY, FAULT ZONE

by

Richard M. D'Angelo

Thesis submitted to the Faculty of the
Virginia Polytechnic Institute and State University
in partial fulfillment of the requirements for the degree of
Master of Science
in
Geophysics

APPROVED:

J. K. Costain, Chairman	L. Glover, III
E. S. Robinson	N. M. Ratcliffe

July 24, 1985

Blacksburg, Virginia

CORRELATION OF SEISMIC REFLECTION DATA WITH SEISMICITY OVER THE RAMAPO, NEW JERSEY, FAULT ZONE

by

Richard M. D'Angelo

J. K. Costain, Chairman

Geophysics

(ABSTRACT)

Reflection seismic data, mylonite reflectivity, gravity data, and earthquake hypocenters have been integrated into a possible explanation for seismicity in the Ramapo fault area. Seven reflection seismic lines were processed using variations in sorting and residual statics. Single VIBROSEIS sweeps were treated as separate sourcepoints. Compressional velocities and densities were determined in the laboratory. Reflection coefficients and gravity models provide evidence for reflections from mylonite zones. Earthquake hypocenters were projected into the vertical seismic sections. The results suggest a correlation between rock volumes containing hypocenters and rock volumes containing mylonite zones. The seismic line furthest from the Taconic suture displays fewer hypocenters and mylonites, in agreement with an assumed model of mylonite development possibly associated with obduction of continental crust. The mylonite zones in the basement may serve as local areas of crustal weakness for seismic activity occurring in the area.

ACKNOWLEDGEMENTS

The reflection seismic data were collected by Virginia Tech as part of a cooperative project with the U.S. Geological Survey, Drs. N. Ratcliffe and J.K. Costain, Principal Investigators. Partial summer support during 1984-1985 was provided by Arco Exploration and Sohio Petroleum Company. Dr. Nick Ratcliffe of the USGS is greatly appreciated for his efforts in obtaining the USGS funds and for the core samples and other valuable geologic information he provided.

I would like to express appreciation to my primary advisor, Professor John Costain for his guidance throughout this project and his valuable comments concerning this manuscript. Professors Lynn Glover, III, Edwin Robinson, Gil Bollinger and Arthur Snoke also provided valuable information and assistance. Additionally, the professional staff of the RGL, , , , , and , and , staff member of the Seismological Observatory, are recognized and thanked for their assistance in their particular areas of expertise. I must have discussed my ideas with all of my fellow students at least once and for their comments and opinions I am thankful, especially .

I owe the educational opportunities I have experienced to the unselfish and unrelenting support and encouragement of my parents. I express the deepest appreciation and love to them. Finally, and most of all, I thank my wife, , for her motivation and constant companionship which keeps my ambition strong and my life complete. To her I dedicate this paper.

TABLE OF CONTENTS

LIST OF ILLUSTRATIONS

LIST OF TABLES

INTRODUCTION

The Ramapo fault zone in the northeastern United States is a portion of an extensive network of northeast trending border faults which generally separate crystalline Proterozoic gneisses and schists to the northwest and Triassic sedimentary rocks to the southeast. According to Ratcliffe (1971) these faults were initially active during the Grenville Orogeny (1 bya) and probably have been reactivated several times through geologic history until the Jurassic (150 mya). Analysis of seismic data has related earthquake locations to the surficial features of the Ramapo fault zone (Page et al, 1968). Interest in better definition of the seismotectonics of this region was spurred by the construction of the Indian Point Nuclear Generating Station south of Peekskill, N.Y., immediately adjacent to a member fault of the Ramapo fault zone (Ossman, unpubl.).

During 1983 and 1984, seven reflection seismic lines were collected by Virginia Tech and the U.S.G.S. in eastern Pennsylvania, northern N.J., and southwest N.Y. (Figure 1). Additionally, velocity and density determinations were made on core samples, and modeling of gravity data was done to interpret the seismic reflections.

PREVIOUS WORK

GEOLOGY

The Ramapo Fault proper extends linearly from Peapack, N.J., about 80 km northeast to Stony Point, N.Y., on the Hudson River (Ratcliffe, 1971). The entire fault system, including splays and branches along strike at both ends of the main normal fault, expands 150 to 175 km. The main extensions are the Canopus Fault system northeast of the Hudson River, and the Flemington-Furlong fault system to the southwest. The trend of the system is approximately N 40° E (Figure 1).

To the northwest of the faults lie primarily Precambrian gneisses (in part the New Jersey and Hudson Highlands) and Cambrian-Ordovician metamorphosed rocks of the Manhatten Prong (Figure 1). This terrane is folded into northeast trending ridges which commonly contain Paleozoic sediments in their intermontane valleys. Also, several mafic intrusives occur ranging in age from Late Precambrian to Late Ordovician-Early Silurian (Ossman, unpubl.). To the southeast, the faults of the Ramapo system generally bound Triassic-Jurassic basin sediments, e.g., the half graben Newark Basin. Many of these Mesozoic basins contain diabase intrusives, such as the Palisades sill.

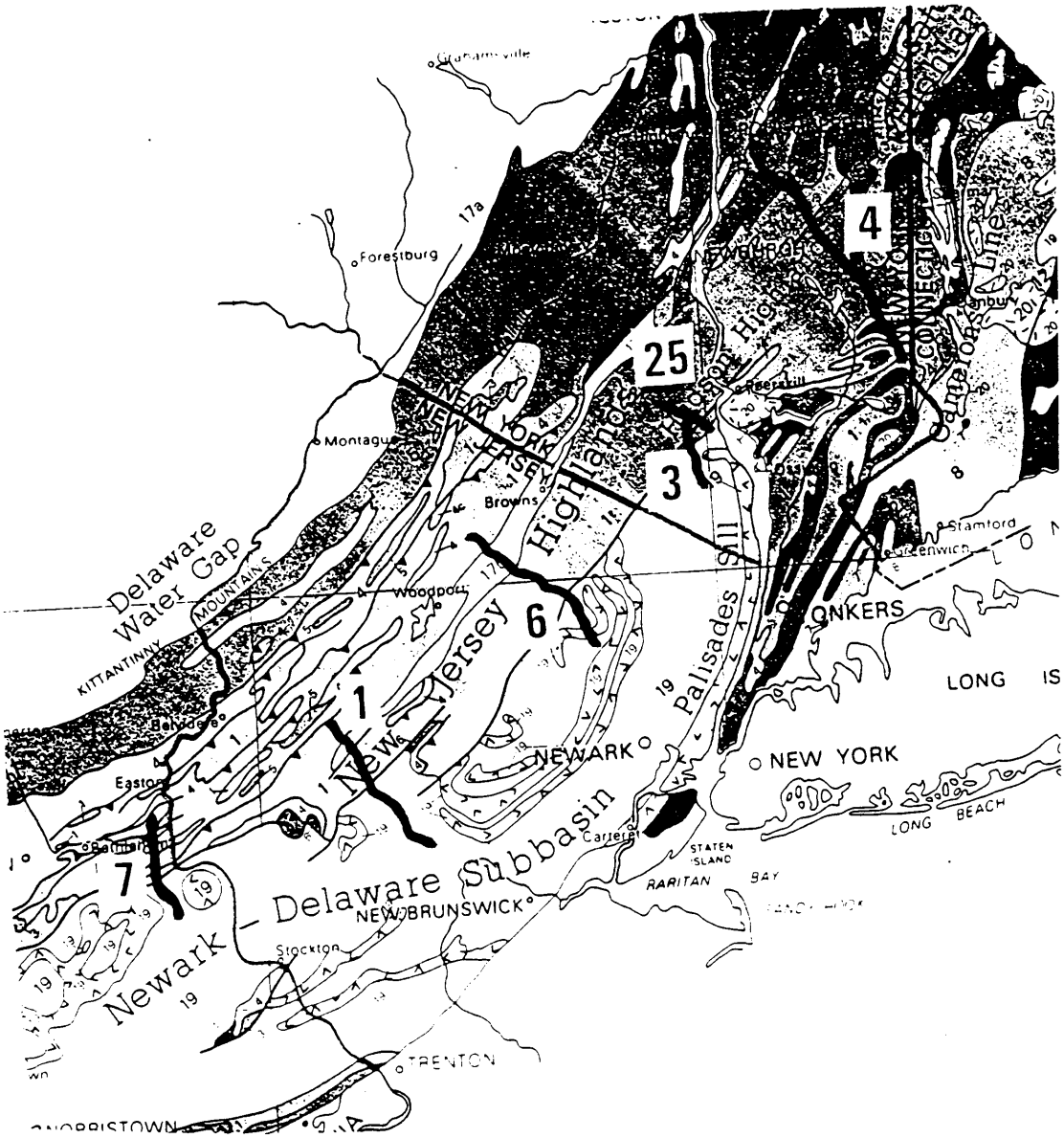

Figure 1. Location map of the seismic lines with the geology of the Ramapo fault zone: Seismic lines are numbered and the geologic data is from the 1978 USGS Tectonic Lithofacies Map of the Appalachian Orogen (compiled by Harold Williams).

Ratcliffe (1976, 1980) recognized two distinct types of faults in the Ramapo system. One is representative of semiductile shear faulting related to major compressive tectonic events; the other is characterized by more brittle fracture (Ossman, unpubl.). The former are older thrust faults associated with mylonite zones, whereas the latter are younger normal or dip slip faults associated with cataclastic fabrics.

The southeast dip of the Ramapo fault and associated faults has been measured by drill hole data (Ratcliffe, 1980). In general, the dips are consistently steeper toward the northeast, ranging from about 45° SE near Riverdale, N.J., to about 70° SE at Stony Point, N.Y.

SEISMICITY

Although the historic record of felt earthquakes in the study area extends back some 250 yrs, only during the last 20 yrs have epicentral locations become accurate enough to be tentatively correlated with geologic structures (Kafka, 1983). Several authors (Kafka, 1983, Kafka et al, 1982, Aggarwal and Sykes, 1978, and Page et al, 1968) suggested that current minor seismic activity may be associated with the Ramapo fault and other exposed northeast trending faults. Some epicenters in the study area appear to be associated with the Ramapo system, occuring within 5 km of a fault with

surface expression (Ossman, unpubl.). However, few earthquakes in the Ramapo fault system area have been convincingly correlated with mapped faults (Fischer, 1981).

Furthermore, the improvement in the determination of focal mechanisms made possible by the increased density of seismic monitoring stations has indicated that recent seismicity is occurring on northwest-trending fractures (Yang and Aggarwal, 1981, and Ossman, unpubl.). Therefore, although some epicenters do occur with an apparent spatial relationship to the faults of the Ramapo system and may indicate movement along these faults, there is a scatter of events throughout the region, and focal mechanism solutions are inconsistent. In addition, no fault displacement or other geologically recent deformation has been observed on faults in the Ramapo fault zone (Ratcliffe, 1980).

REFLECTION SEISMIC DATA ACQUISITION AND PROCESSING

DATA ACQUISITION

All RAMAPO lines were acquired by personnel from the Regional Geophysics Laboratory (RGL) of the Geological Sciences Department at Virginia Tech using a single Failing Y-1100 P-wave vibrator. Min-Max 10-Hz geophones were used in Chebychev weighted 20-element arrays in conjunction with an MDS-10 48-channel digital recording system with field summing capability. Figure 1 is a location map of the seven lines and Table 1 shows the recording parameters for the lines. Additional recording parameters are given in Appendix A.

Data acquisition in this densely populated urban corridor is difficult. For example, during the data collection along Line 5, cultural obstacles necessitated the shooting of several consecutive vibrator sweeps at the same location. The inconsistent manner in which these data were collected caused many of the CDPs to contain several traces with the same offset, falsely biasing the data. These repeated common-offset traces were edited out during processing.

Table 1. Data recording parameters for the seismic lines

LINE NAME	LINE1	LINE2	LINE3	LINE4	LINE5	LINE6	LINE7
DIRECTION SHOT	SE to NW	SE to NW	N to S	SE to NW	SE to NW	NW to SE	SE to NW
FOLD	12	12	12	12	24	12; 24	12; 24
CDP SPACING (m)	34.5	34.5	34.5	34.5	17.25	34.5	34.5
NUMBER OF SHOTS	234	47	73	330	113	186; 63	35; 146
LINE LENGTH (KM)	32.3	6.5	10.1	45.5	3.9	30.3	15.0
RECEIVER PATTERN							
GROUP INTERVAL (m)	69	69	69	69	34.5	69	69
PATTERN (offend)	PULL	PULL	PULL	PUSH	PULL; PUSH	PULL	PUSH
NEAR/FAR OFFSETS (m)	417/3684	417/3684	417/3684	348/3614	variable	348/3614	348/3614
SOURCE PATTERN							
NUMBER OF VIBRATORS	1	1	1	1	1	1	1
GROUP INTERVAL (m)	138	138	138	138	34.5	138; 69	138; 69
ARRAY LENGTH (m)	69	69	69	69	69	69	69
SWEEPS/VP (sum?)	16; 12(no)	12 (no)	12 (no)	16; 12(no)	16; 8 (no)	16 (yes)	16 (yes)
SWEEP FREQUENCY (Hz)	14 to 56	14 to 56	14 to 56	14 to 56	14 to 56	14 to 56	14 to 56
SWEEP LENGTH (sec)	24; 30; 27	27	27	27	27	24	24
RECORDING TIME (sec)	29; 35; 32	32	32	32	32	29	29
DATA LENGTH (sec)	5	5	5	5	5	5	5
SAMPLE RATE (sec)	0.002	0.002	0.002	0.002	0.002	0.002	0.002

DATA PROCESSING

All processing was done at the RGL on a Digital Equipment Corporation (DEC) VAX 11/780 computer, Floating Point Systems (FPS) 120B array processor, and Digicon DISCO seismic software. All lines have undergone the same standard processing routine as described in Appendix B. In addition, several unusual techniques were used. For example, the effects of different CDP line orientations and the application of iterative automatic residual statics and time-variant automatic residual statics were investigated. Furthermore, Lines 1, 2, 3, and 5 were subject to single-sweep processing.

CDP LINE ORIENTATION

During CDP sorting the effects of different CDP line orientations were investigated. In a normal common-depth-point (CDP) sort, a line of CDP stations (surface locations) is defined that is coincident with the source-receiver stations but with a spacing half that of the latter. Each trace is then assigned to the CDP station nearest to the source-receiver midpoint location. This is done under the assumption that all energy on the trace was reflected from a subsurface point located at the source-receiver midpoint. All traces assigned to a CDP station are then gathered (sorted) and summed (stacked) to form a single trace which (using the above assumption) contains all the recorded energy

which was reflected from beneath the CDP station. This assumption is reasonable for horizontal reflectors; for dipping events it is not valid.

In the case of an inclined interface and a straight line, energy reflected from different parts of the reflector will be included in the CDP gather, but the reflection time will still vary systematically as a function of offset. The result is that the reflector will be imaged at an artificially high stacking velocity (Levin, 1971).

Where crooked roads and dipping interfaces are encountered, reflections from different depths along the inclined reflector are again collected into the same stacking gather. Unfortunately, because of erratic road geometry (and resulting erratic apparent reflector dip), the reflection time will not be a simple function of its source-receiver offset and the reflector will not be imaged at any stacking velocity.

In the RAMAPO lines the roads were mostly crooked. To properly image dipping reflectors, a method of gathering the data parallel to geologic strike was employed. A CDP line was defined perpendicular to geologic strike, and the data were gathered perpendicular to this line. Thus, the data were essentially projected onto the contrived CDP line and each CDP gather contained all the traces with midpoints at the same relative dip locations.

This process acts as a dip filter for which only interfaces with a dip direction near that of the CDP line will be

properly imaged. This filtering effect is also present in a normal CDP sort; however, the erratic CDP line caused the dip filter to change direction depending upon the road direction, often within one receiver array length. The projection technique merely allows a choice of dip direction (it must be nearly the same direction as the line, however, to keep a reasonable fold and line length).

RESIDUAL STATICS

Static corrections were found to be a major problem on all of the Ramapo lines. Datum static corrections, followed by extensive surface consistent residual static corrections were applied to the data. The residual statics were computed in an iterative manner; a velocity function was chosen, residual statics applied, then often another velocity analysis was done and the velocity function revised if necessary. This sequence was repeated several times, usually three or four, on most lines to optimize the statics used for the final sections by accumulating the calculated values after each run.

An unconventional time-variant residual statics calculation also was applied to some of the lines, a procedure beyond the capability of the DIGICON software, by processing the data twice, first applying ARS to the shallow part of the section and a second time by applying ARS to the deeper part of the section. The two output data sets were muted to

'zero-out' the portion not subjected to the ARS routine, and then summed, resulting in a complete section that has had different automatic residual statics computed for the shallow and the deep portions.

SINGLE-SWEEP PROCESSING

The standard reflection seismic data acquisition technique used involves the summation of commonly 16 or 12 VIBROSEIS sweeps symmetrically located around a common shot point. This summation occurs in the field or after correlation and is disadvantageous because the structural detail along the summation distance is lost. However, for single-sweep processing, the individual sweeps are not summed, but are recorded separately and continue through the entire processing sequence as separate sources. By recording and processing the sweeps individually, greater lateral resolution is apparent in the final section (Belcher, unpubl.). This procedure was applied to Lines 1, 2, 3, and 5.

During single-sweep processing each VIBROSEIS sweep is treated as a separate shot point with the receiver array held constant for each 'family' of 16 or 12 sweeps. Thus, although the distance the reflection line covers remains the same, the effective length of the section is increased by a factor of 16 or 12. The appearance of reflectors is distorted as dipping beds are stretched out severely and appear flat.

Station locations for the individual sweeps are interpolated by assuming the sweeps are spaced at constant intervals equal to the station spacing (69 m) divided by the number of sweeps per shot point (16 or 12). Therefore, the CDP spacing for the single-sweep sections is about 2.2 m for 16 sweeps/shot and about 2.6 m for 12 sweeps/shot; the shot spacing is approximately twice this value.

DISCUSSION

PROCESSING

Common depth point sorting along crooked survey lines results in stacked sections with highly variable fold coverage. Thus, best-fit modified-crooked CDP sort lines often are defined along crooked survey lines. However, because the orientation of the CDP-line can act as a dip filter, several different CDP-line orientations were used to sort each of the Ramapo lines and the resultant stacked sections were compared.

The Ramapo lines are oriented generally NW-SE, approximately perpendicular to surface geologic strike. The stacked sections of the lines submitted to standard processing appear in Appendix D. All have been sorted using a modified-crooked CDP-line definition and plotted with no vertical exaggeration. A difference in the stacked section caused by CDP-line orientation was observed for Line 3. Unlike the other lines, Line 3 is oriented oblique to surface geologic strike. Thus, the best-fit modified-crooked CDP-line also is oriented oblique to surface geologic strike. A straight CDP-line oriented perpendicular to geologic strike was defined for this data in order to sort traces from common depths on a dipping reflector. The stacked section shows a

different perspective of the border fault and Triassic basin than the original section (Figure 2).

Less significant differences (if any) were observed for the other lines. For example, Line 6 has an abrupt change in direction as it crosses the surface trace of the border fault. This orientation was considered a possible reason for the lack of coherent reflected energy from the subsurface fault plane on the modified-crooked line section. However, when sorted along a straight CDP-line perpendicular to the surface trace of the fault, the resulting stacked section still did not contain reflections from the buried fault plane (Appendix E).

The single-sweep data also were processed using different CDP-line orientations. Crooked-line, modified-crooked line, and straight-line CDP sorts were performed on the data. As opposed to the standard data, the straight CDP-line defined perpendicular to strike was observed to produce a single-sweep stacked section with the best coherency and most constant fold coverage. Therefore, the single-sweep sections also offer a different perspective of the data. For example, part of Line 1 was processed single-sweep and then summed after processing for comparison on the same scale with the standard data (Figure 3). Note the possible indication of a fault on the summed single-sweep section which is not present on the standard data. This observation may be due to either

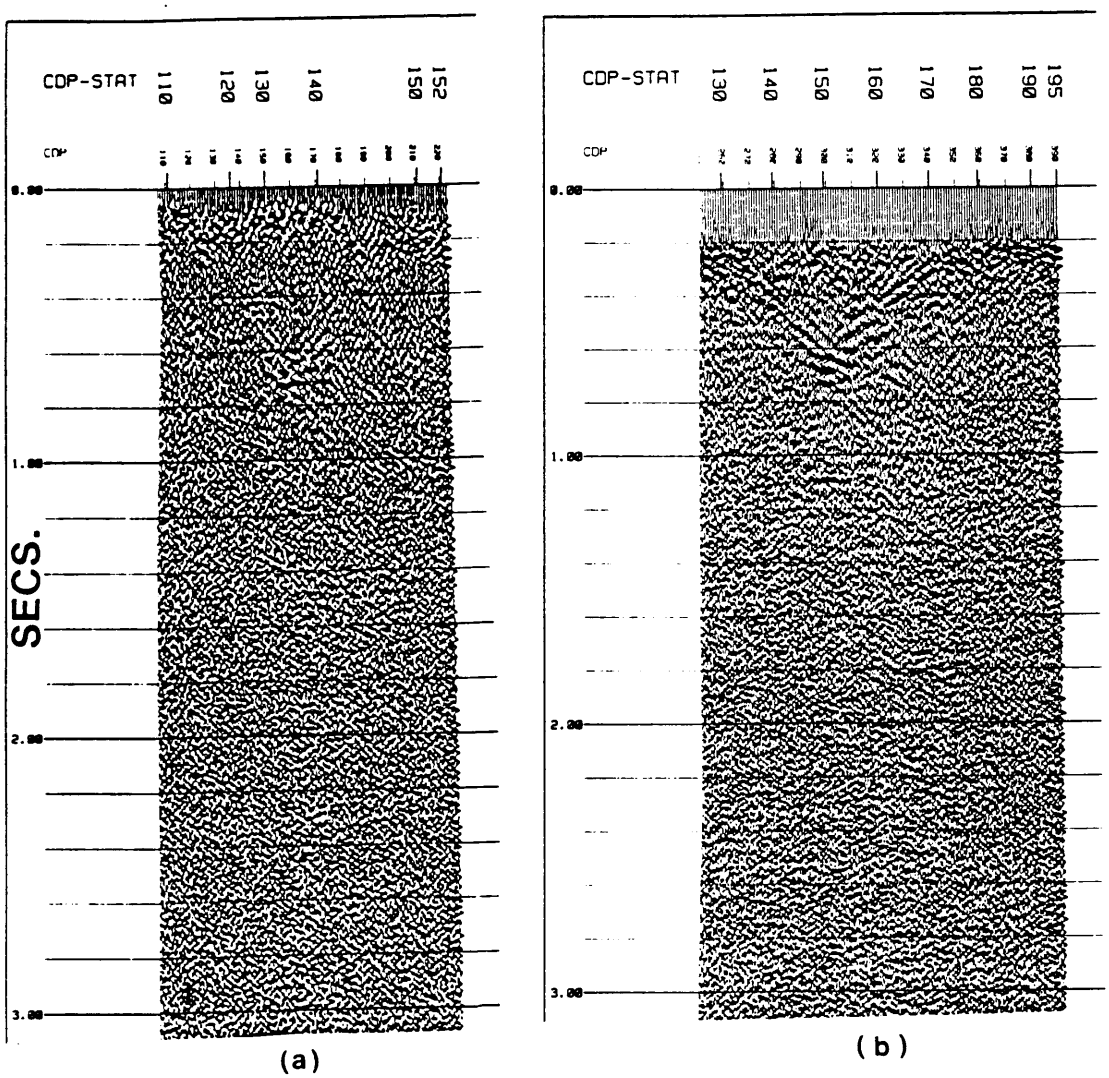

Figure 2. Effect of CDP line orientation on Line 3: Part of Line 3 containing reflection from the border fault (a) sorted with a straight CDP line perpendicular to strike and (b) sorted with a modified-crooked CDP line oblique to strike. (Unmigrated and no vertical exaggeration)

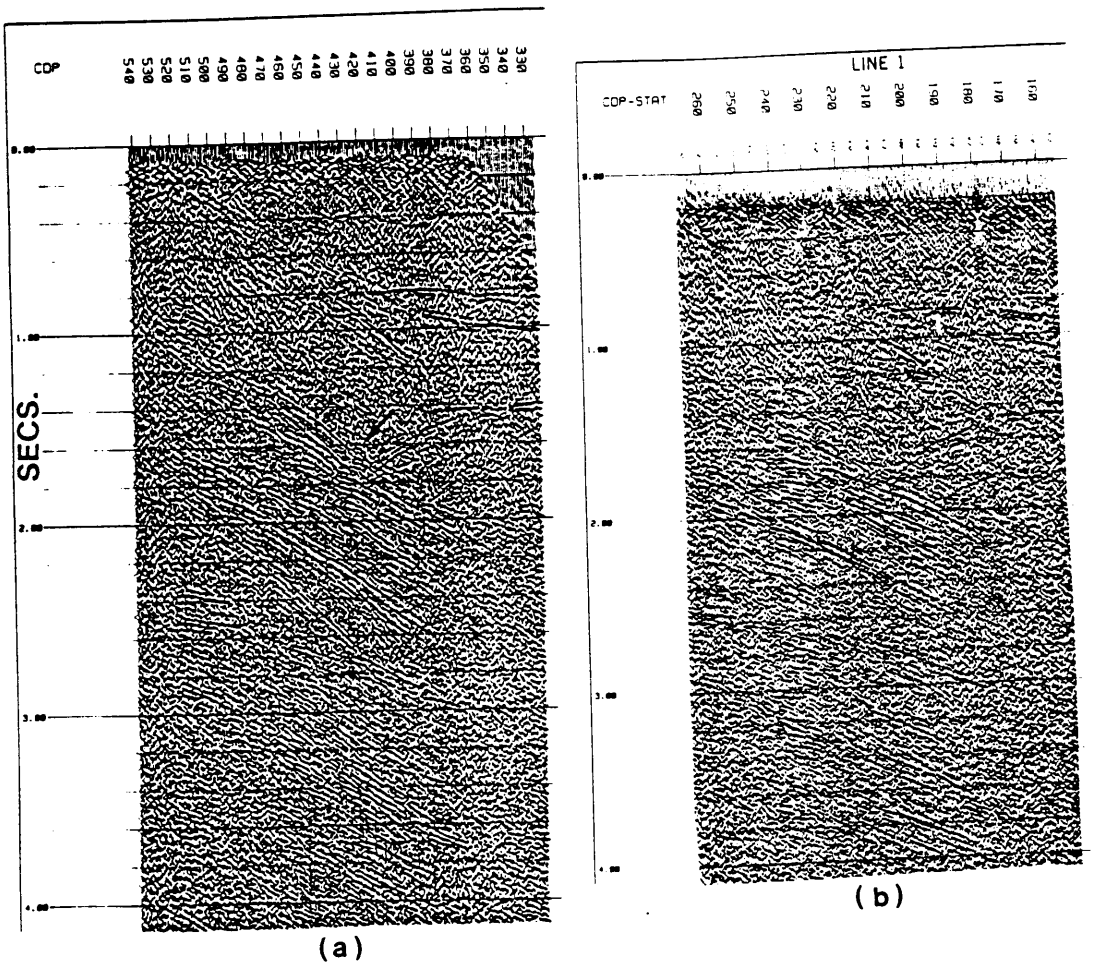

Figure 3. Summed single-sweep processing vs. standard processing for Line 1: (a) Part of Line 1 processed by single-sweep and summed. Note possible fault location marked by arrow that is not apparent on the standard section of Line 1 (b) and the increased coherency of reflection 'I' on the single-sweep data. (Unmigrated and no vertical exaggeration.)

the different orientations of the CDP lines or to the process of single-sweep processing.

Automatic residual statics (ARS) calculations are applied to correct for shifts in the data that are not removed by datum statics corrections. Static shifts were limited to 20 ms. These corrections were especially valuable due to the low fold coverage (12 to 24) and low signal-to-noise ratio of these data. In particular, deep coherent energy from within the crystalline basement was greatly enhanced by the application of ARS. A good example of this effect can be observed on the data from Line 4 plotted before and after ARS calculations (Figure 4). Note the increased coherency of the reflections after application of residual statics calculations. Line 4 is located largely over Precambrian crystalline rocks and required three iterations of the ARS routine to obtain this improvement. Similar reflection enhancement is observed on data from Line 6 (Appendix E).

Line 7 (Figure 5) and Line 25 (Appendix E) were subject to time-variant residual statics corrections also resulting in enhancement of reflections from within the basement. This process enables corrective shifts to be applied to deep reflections without degrading the coherency of shallower reflections.

The presence of signal coherency within the crystalline basement rocks is evident to some degree on all of the Ramapo lines (Figure 6). The application of residual static cor-

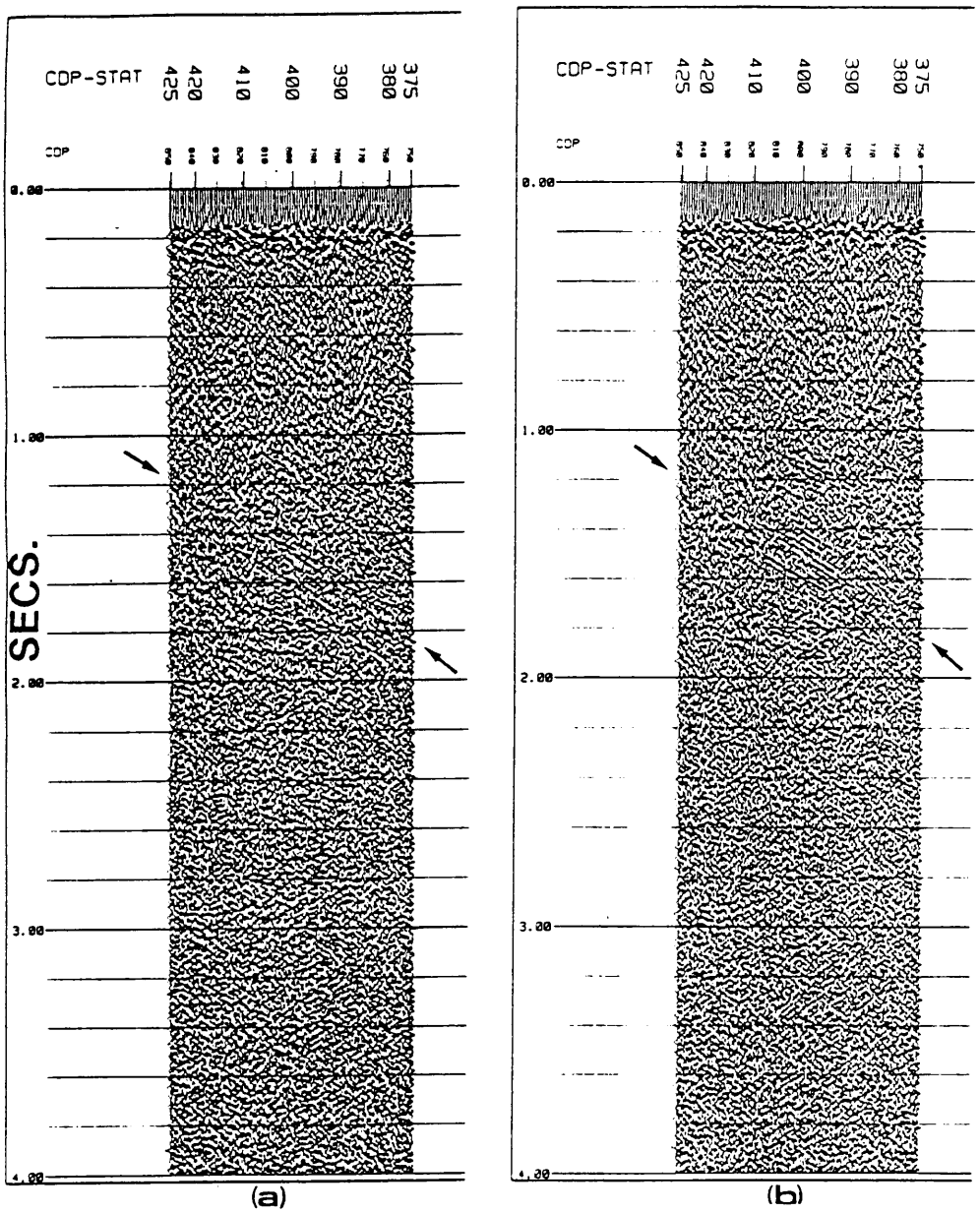

Figure 4. Part of Line 4 before (a) and after (b) application of residual statics corrections: Note the effect on the reflections marked by the arrows. (Unmigrated and no vertical exaggeration.)

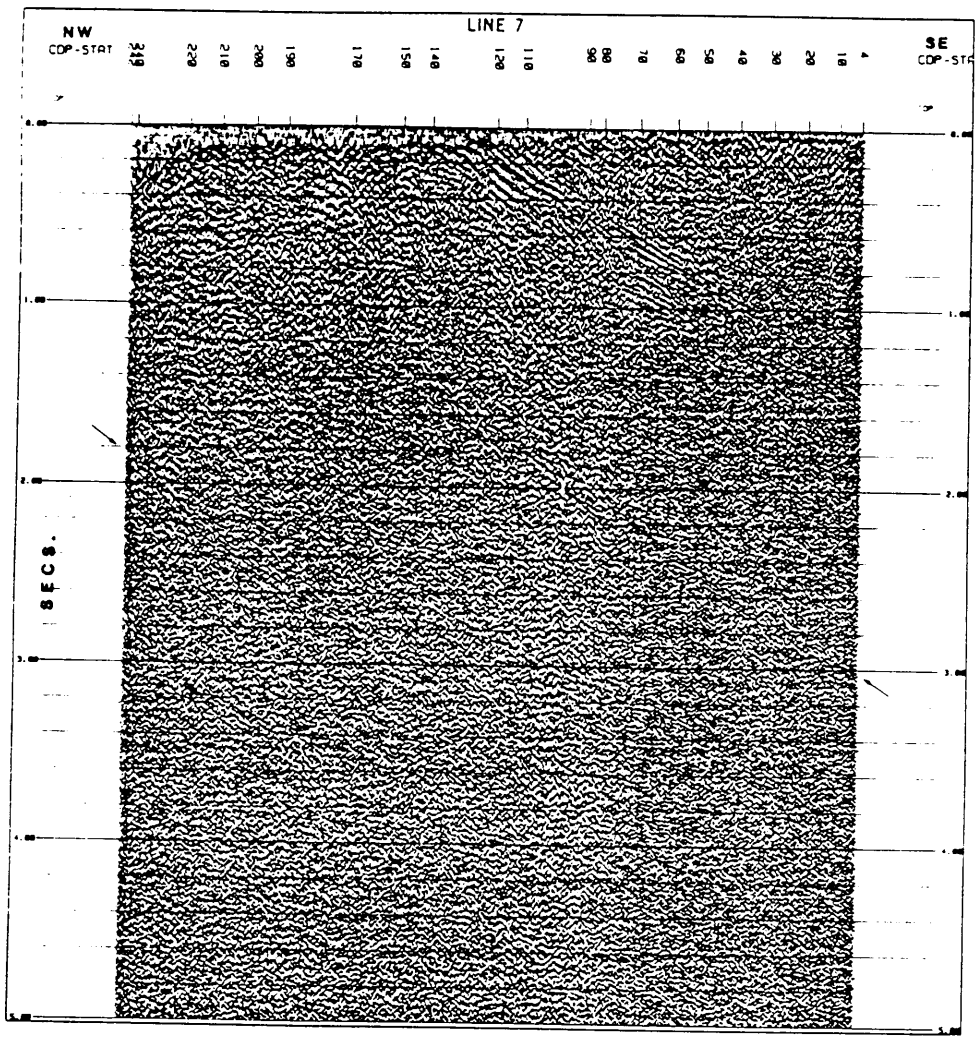

Figure 5. Line 7 with time-variant ARS: Enhanced signal coherency marked by arrows. (Unmigrated and no vertical exaggeration.)

rections improved this coherency. However, it was observed that for this data the ARS software will not cause alignment of reflection amplitudes (coherency) where signal coherency is not already present. That is, the residual static corrections affect enhancement of preexisting coherency in the data but do not produce artificial coherency where none previously exists.

Single-sweep processing was performed on Lines 2, 3, 5 and part of Line 1. Reflections from the bottom of the basin on Line 3 (Figure 7) appear offset indicating small, near-vertical (about 80°) thrust(?) faults in the basement. Evidence for these faults is not apparent on the standard section of Line 3. Also on Line 3 near surface reflections, possibly indicating another shallow basin, were observed on the single-sweep data (Appendix E) but not on the standard data.

Similarly, improved geologic information was available from the single-sweep sections of the other lines. For example, a reflection on the single-sweep section of Line 5 (Figure 8) has much greater lateral continuity and coherency than is observed on the standard section. In fact, on the single-sweep section this reflection resembles the interpreted mylonite(?) reflections observed on the other lines, discussed later.

All of the single-sweep stacked sections were summed after complete processing for further comparison with the

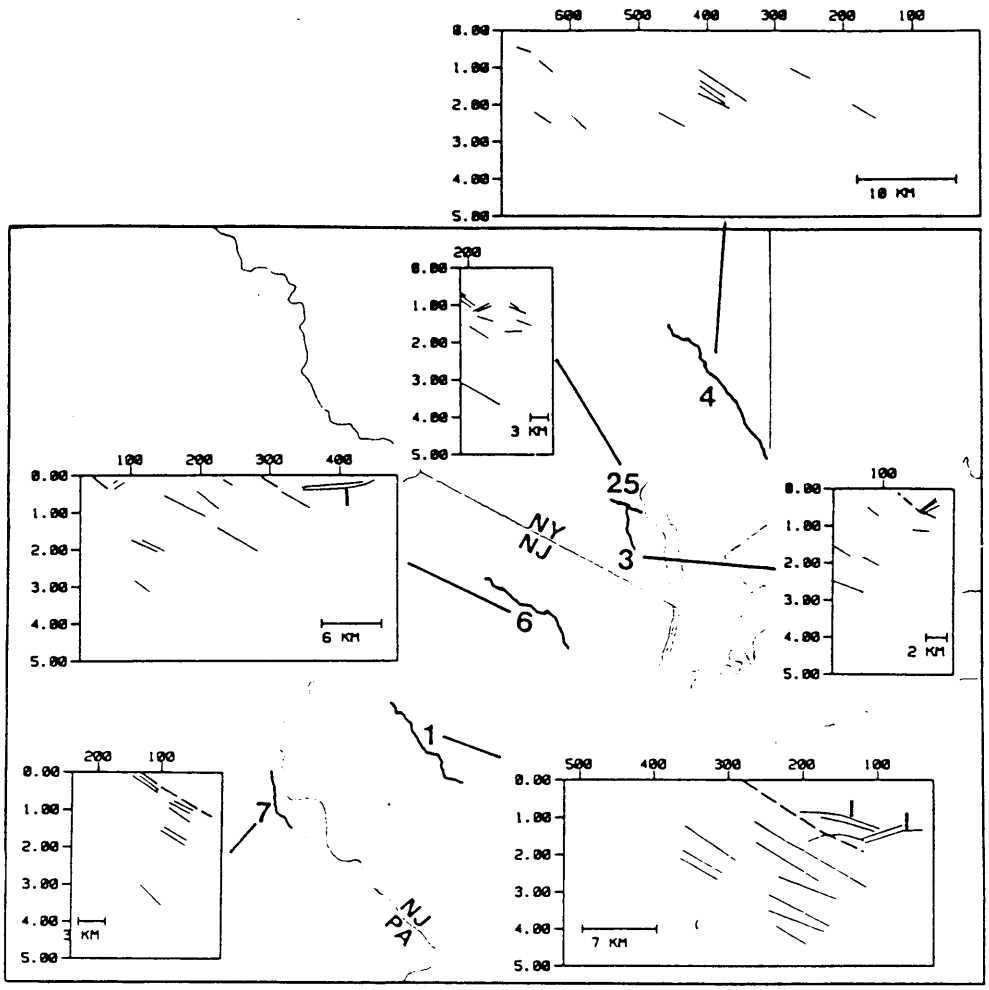

Figure 6. Fence diagram with line drawings of the seismic sections: All sections are at the same scale with no vertical exaggeration. Vertical axes are two-way travel times in seconds and horizontal axes are surface stations. Dashed lines represent border fault reflections. Some reflections from within the basins are interpreted to be from igneous intrusives (labeled 'I'). Unlabeled reflections are interpreted to be from mylonite(?) zones.

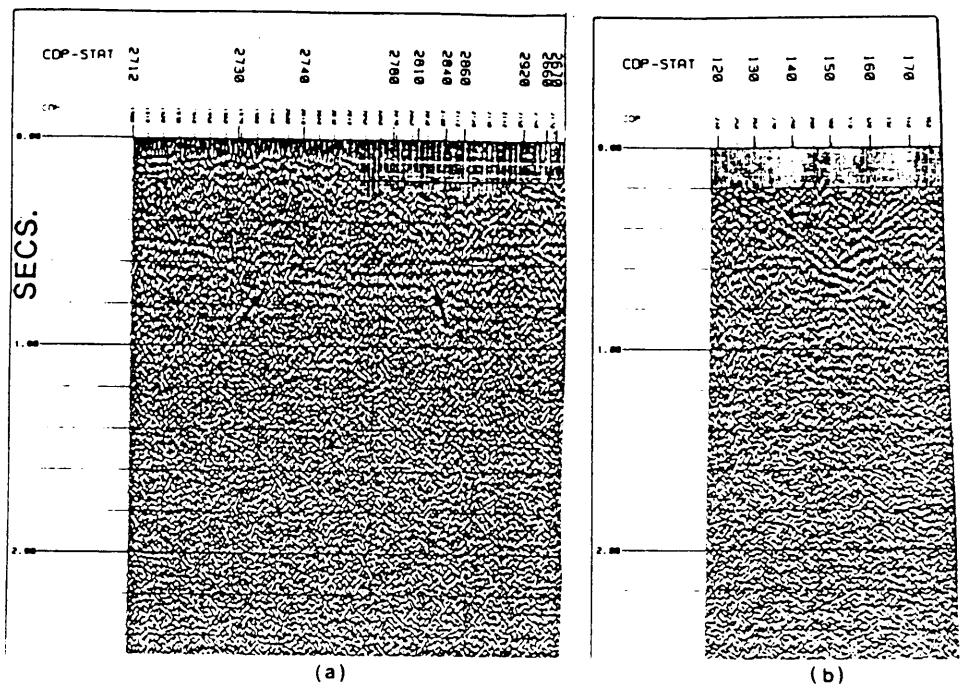

Figure 7. Single-sweep processing vs. standard processing for Line 3: (a) Part of line 3 single-sweep section. Note the indications of offsets in the bottom of the basin (marked by arrows). (b) Basin reflections from standard section with no apparent offsets. (Unmigrated)

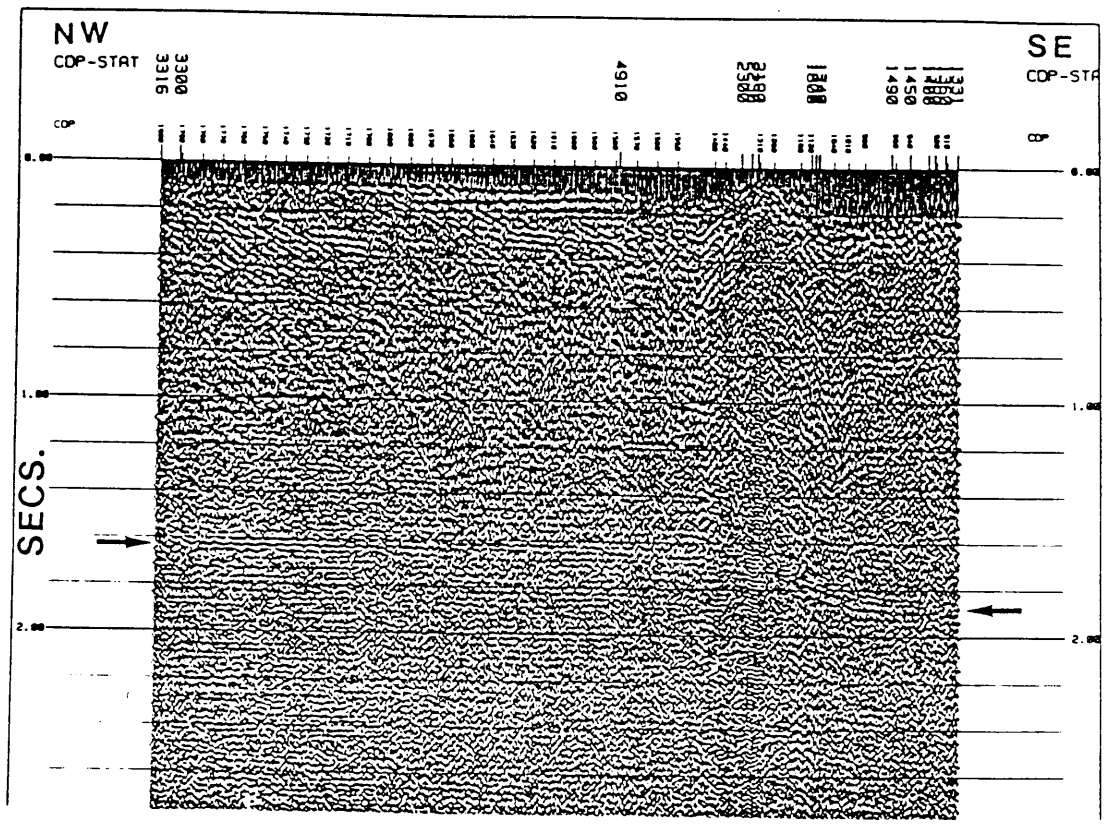

Figure 8. Line 5 single-sweep section: Note the strong continuous reflection marked by the arrows. Doming of traces around CDP 1310 due to irregular data collection. (Unmigrated)

standard sections. The increased coherency and increased signal-to-noise ratio on the single-sweep data of Line 1 is especially well illustrated in this manner. For example, reflection 'I' on Line 1 is a more laterally continuous event on the single-sweep data than on the data stacked in the conventional manner (Figure 3). This same enhancement of reflections is observed on other summed single-sweep sections (Figure 9 and Figure 10).

VELOCITIES, DENSITIES, AND REFLECTION COEFFICIENTS

Reflections from the border faults and intrusives within the Triassic basins have been interpreted by their correlation with surface geology (Figure 6). Interpretation of the reflections from deep within the basement is supported by the following analysis. Density and ultrasonic velocity determinations were made on core samples (Table 2) from the U.S.G.S. drill-hole at Rattlesnake Hill near Riegelsville, Pennsylvania (proximal to Line 7, Figure 13) and the Letchworth #2 drill-hole near Annsville, New York (proximal to Line 25). The dip of the mylonitic fabric in the Rattlesnake Hill core was between 20° and 30°, whereas it was about 70° in the Letchworth core. P-wave velocities were measured parallel to the axis of the core, except for sample L2 for which the velocity was measured perpendicular to the mylonitic foliation. Velocity determinations were made at

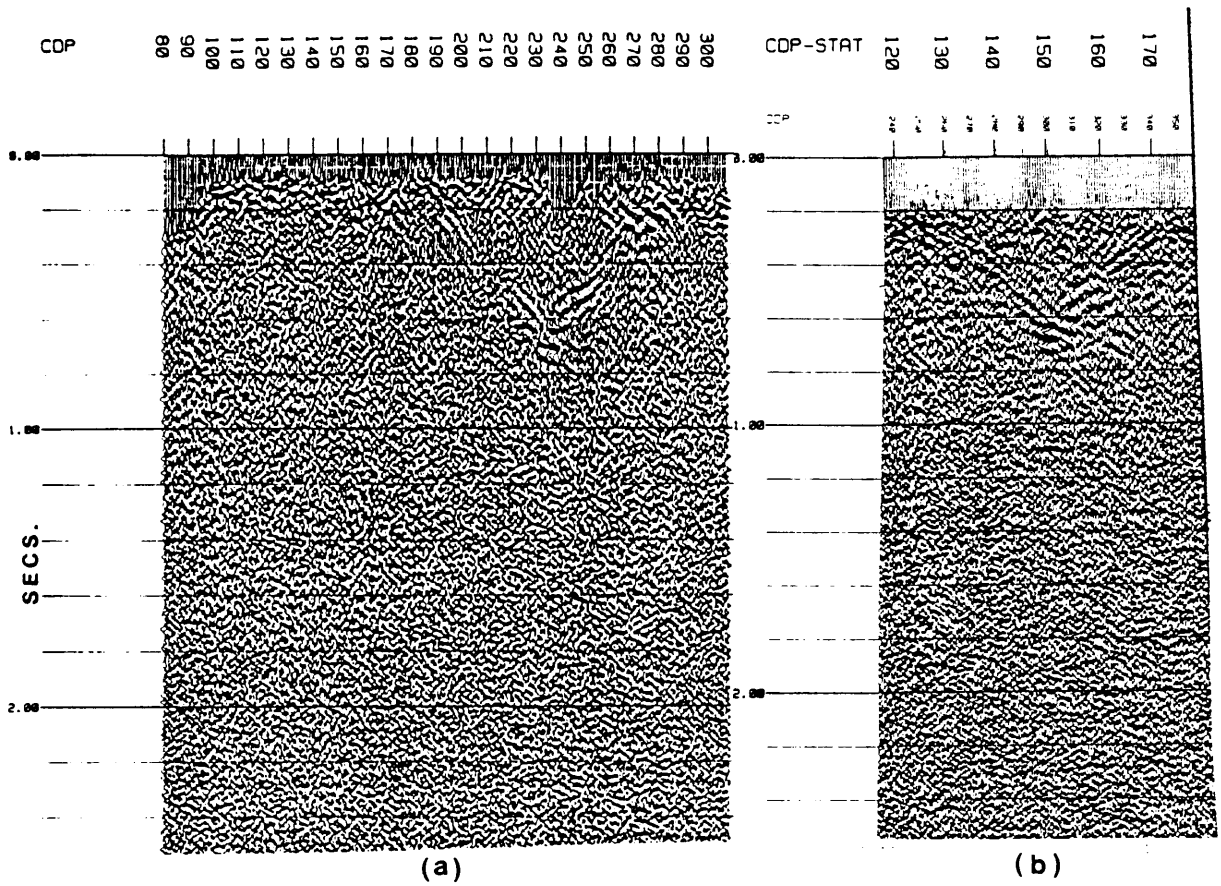

Figure 9. Summed single-sweep processing vs. standard processing for Line 3: (a) Summed single-sweep data of Line 3 and (b) part of standard section. (Unmigrated and no vertical exaggeration)

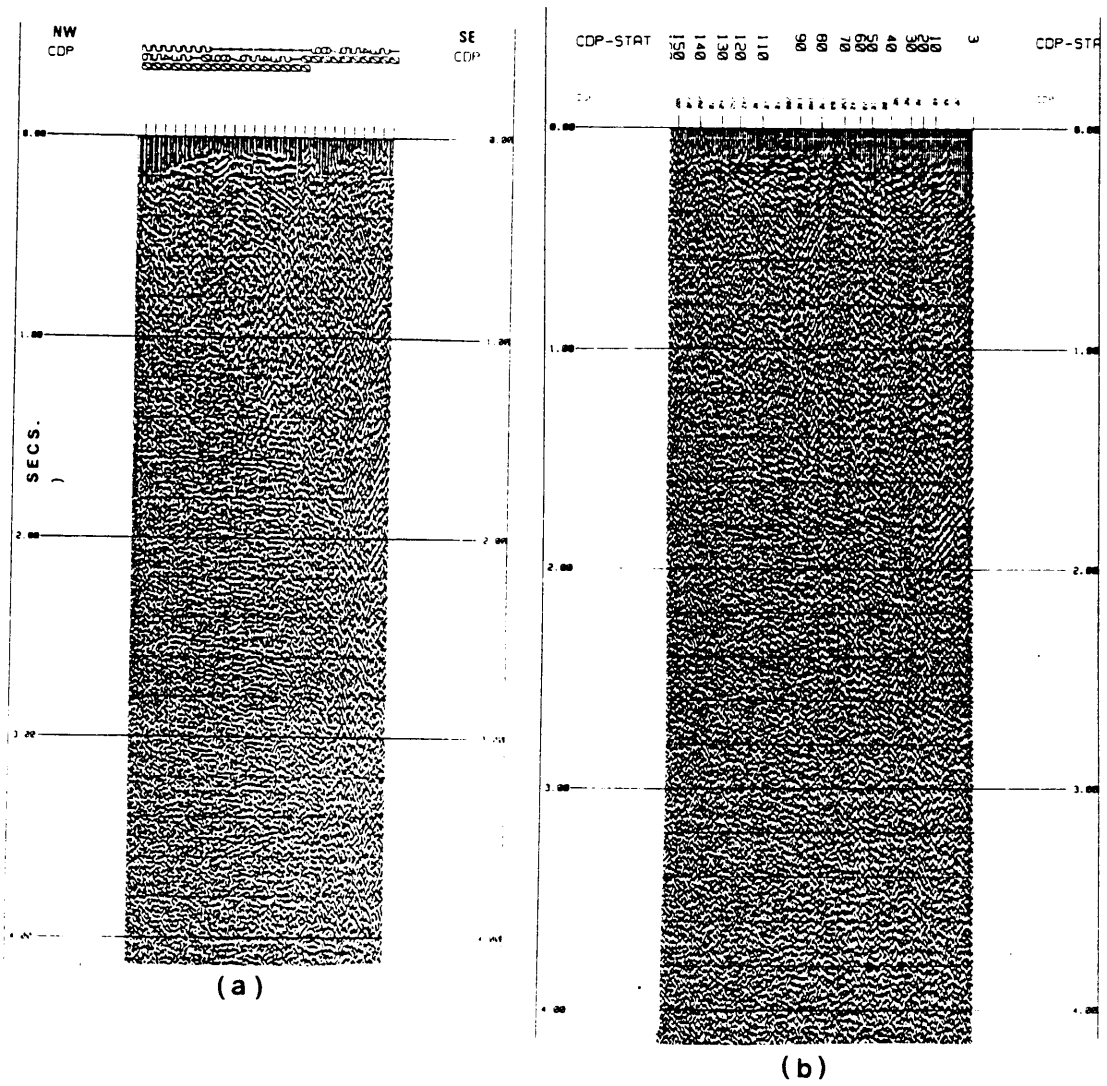

Figure 10. Summed single-sweep processing vs. standard processing for Line 5: (a) Summed single-sweep data of Line 5 and (b) corresponding part of standard section of Line 25. (Unmigrated and no vertical exaggeration)

lithostatic pressures between 500 PSI and 9000 PSI. Density and velocity determinations were performed twice. The densities (Table 2) and p-wave velocities (Figure 11) are close to published values for similar rock types (Jones and Nur, 1984, and Telford at al, 1976). Because of the small size of the sample used to measure the velocity of p-waves propogating perpendicular to foliation (sample L2), the error in these values is about 11%, i.e., as much as plus or minus 500 m/s. Velocities for waves traveling parallel to the mineral foliation could not be measured because the samples shattered along the foliation planes under relatively low pressures (<500 PSI). Reflection coefficients (Table 3) were calculated assuming a normal incidence raypath (Neidell, 1984),

$$\frac{\rho_2 V_2 - \rho_1 V_1}{\rho_2 V_2 + \rho_1 V_1} (\cos \theta)$$

where $\theta = 90°$ is the angle of incidence of the raypath. The high reflection coefficients (absolue value) between the mylonitic and non-mylonitic rock layers (>0.1) may be indicative of reflections from mylonite zones. Reflection coefficients of 0.14 and 0.125 are good reflectors (Neidell, 1984).

Specifically, for seismic energy propogating through homogeneous undeformed basement adjacent to a deformed mylonitic zone with a propogation direction perpendicular to the foliation in the mylonites, a large enough acoustic

impedance contrast would exist to cause a detectable seismic reflection. Therefore, the reflections from deep within the basement are asserted to be from mylonite zones. Another proposed explanation for these reflections is basaltic intrusives. However, the type of basaltic formations necessary are not observed on the surface as is the widespread occurrence of mylonite and shear zone outcrops.

Table 2. Rattlesnake Hill(RH) and Letchworth(L) core samples with depths of occurrence in meters and measured densities in gm/cm^3 (errors < 0.5%).

SAMPLE-DEPTH	LITHOLOGY	DENSITY
RH1-31	hornblende gneiss	2.73
RH2-116	mylonitic hornblende gneiss	2.67
RH3-126	dolomite/dolomitic limestone	2.88
RH4-202	mylonitic limestone	2.80
RH5-251	homogeneous gneiss	2.67
L1-159	homogeneous granite	2.68
L2-41	mylonitic granite(?)	2.63

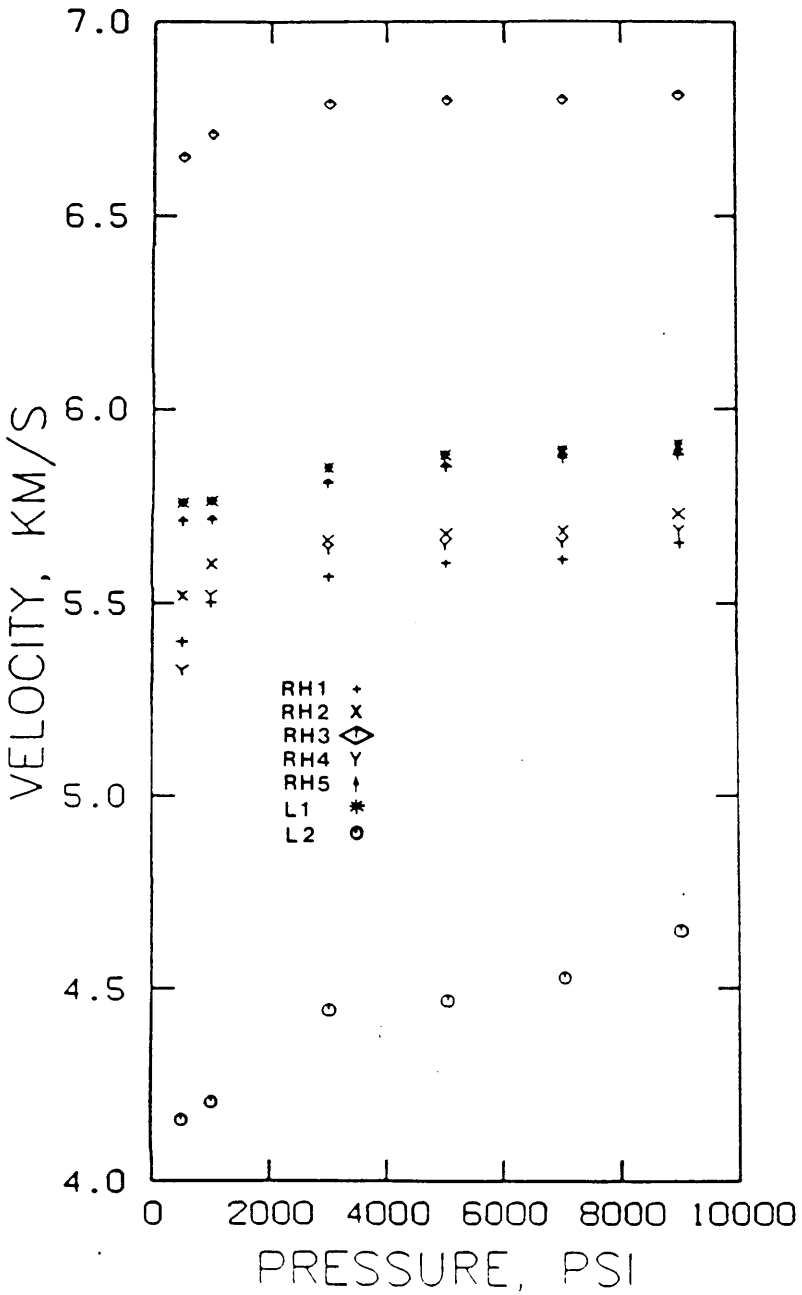

Figure 11. P-wave velocities (km/s) of core samples at various lithostatic pressures: An approximately 3% to 4% error is inherent, i.e., plus or minus 200 m/s. Somewhat higher for sample L2 (see text).

Table 3. Reflection coefficients at various pressures.

CORE SAMPLE	500 PSI	1000 PSI	3000 PSI	5000 PSI	7000 PSI	9000 PSI
RH1						
	-0.001	-0.003	-0.004	-0.005	-0.006	-0.006
RH2						
	0.130	0.127	0.127	0.127	0.126	0.123
RH3						
	-0.123	-0.110	-0.105	-0.105	-0.105	-0.103
RH4						
	0.010	-0.008	-0.010	-0.008	-0.006	-0.008
RH5						
L1						
	-0.170	-0.165	-0.145	-0.145	-0.140	-0.128
L2						

GRAVITY DATA

Additionally, evidence for the possibility of reflections from mylonite zones is derived from analysis of gravity data in the study area. The origin of the gravity field over orogenic terranes has been the subject of many papers (Turcotte and Schubert, 1982, Watts, 1981, Simpson et al, 1981, Griscom, 1963, Zietz et al, 1963, Airy, 1855, and Pratt, 1855). The Bouguer gravity anomalies observed over the Appalachian and other mountain systems such as the Alps and Himalayas consist of a large-amplitude positive and negative gravity anomaly. Brooks (1970) related the anomaly couple to the overthrusting of one crustal plate onto another. In his interpretation the outer gravity high is related to the lithospheric flexural bulge (the topography) and the outer gravity low is related to the basement deformation caused by the surface load. Karner and Watts (1982) described a modified version of such a model which includes the effects of subsurface loading.

Karner and Watts (1982) suggest that any load acting on the lithosphere will be associated with a positive gravity anomaly, i.e., undercompensation. Therefore, a second inner gravity high in the Bouguer anomaly profile over the Appalachians not related to the lithospheric flexural bulge may indicate the existence of some other load acting upon the lithosphere in addition to the surface topography. They

propose that the observation that the peneplanation of the Appalachians has not resulted in the destruction of its molasse basin is evidence for the existence of a subsurface load that is not expressed in the topography. Thus, the validity of their model rests on the assumption of a surface loading (fold/thrust belts) as well as a subsurface loading (obducted blocks/flakes). It is the subsurface crustal loads which may be responsible for the additional inner positive anomaly observed on the Bouguer gravity profiles over the Appalachians.

The model of Karner and Watts (1982) consists of the obduction of continental crust onto a broken elastic plate (Figure 12). The model implies that the strongly asymmetric negative component of the anomaly is related to the deformed basement and the symmetric positive component is associated with subsurface crustal loads. This simple model agrees well with observed data over the Appalachians (Karner and Watts, 1982). The gravity anomalies over the Himalayas and Alps also can be described by flexure due to surface and subsurface loads (Karner and Watts, 1982). With regard to the present study, the edge of the obducted broken plate is coincidental with the steep gravity gradient of the inner positive anomaly. Therefore, the edge of the broken plate and thus, the Taconic suture zone may be delimited by the observed inner gravity anomaly high.

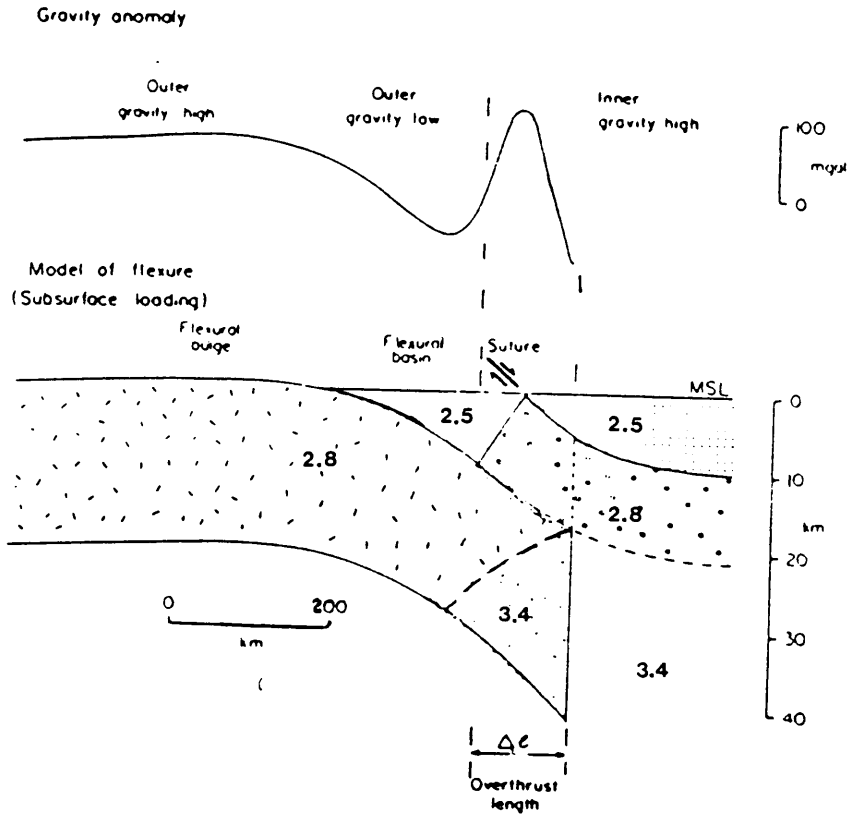

Figure 12. Subsurface loading model: Calculated gravity effect and flexure profile for subsurface loading using a broken plate. Densities are given. (From Karner and Watts, 1982)

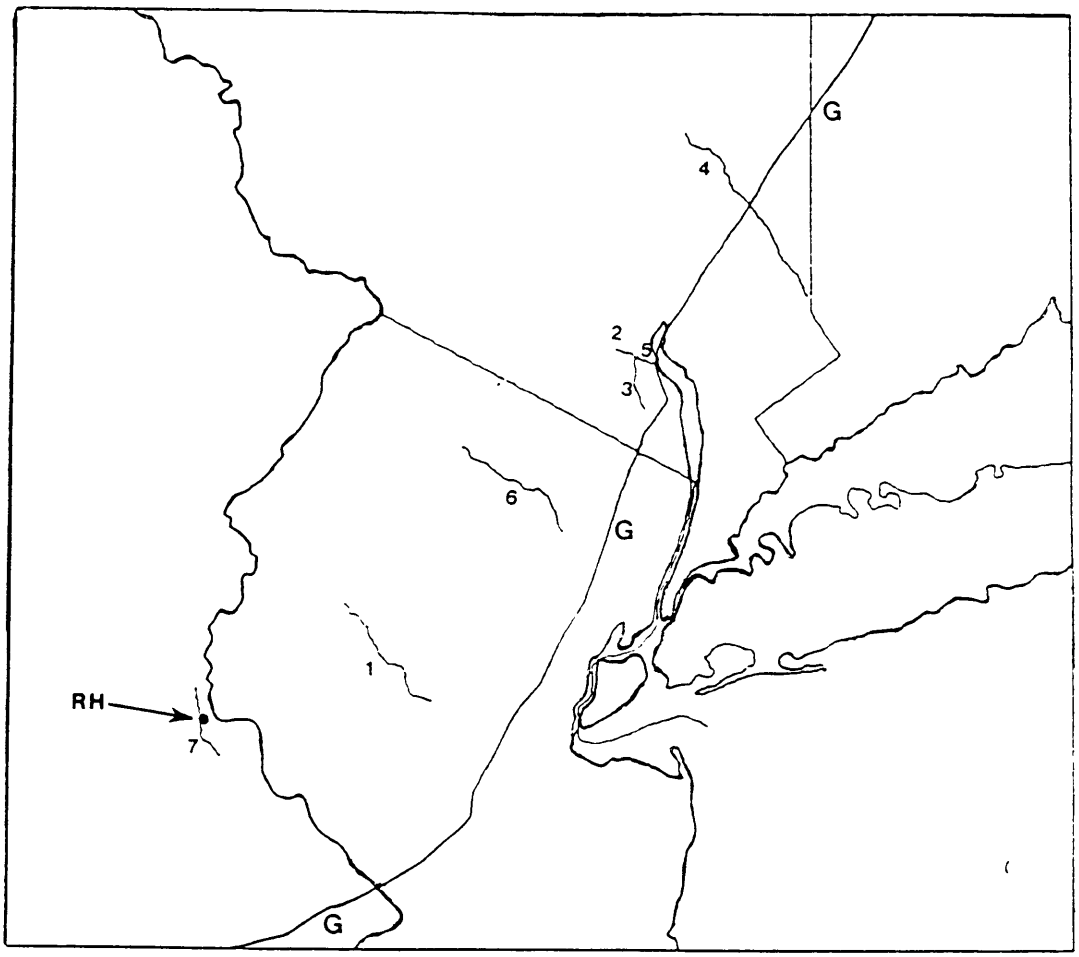

Figure 13. Seismic lines and the general trend of the steep gradient of the Bouguer gravity anomaly field: The seismic lines are numbered and line 'G' marks the area of the inflection in the gravity gradient from the 1982 SEG gravity map of the U.S. The approximate location of the Rattlesnake Hill drill-hole is indicated by point 'RH'.

The steepest part of the gradient in the Appalachian Bouguer gravity field from the 1982 SEG gravity anomaly map of the U.S. is located just east of all of the Ramapo lines except Line 4 (Figure 13). Assuming the gravity gradient does mark the suture zone formed during the Taconic orogeny, then it is evident that the suture zone and thus the basement to the east will not be imaged on six of the seven vertical seismic sections. Yet, the absence of the suture zone does not preclude the appearence of related ductile deformation zones (mylonite zones) on any of the seismic lines. For example, a Bouguer gravity anomaly profile parallel to Line 1 has been modeled using a modification of the Karner and Watts (1982) model (Figure 14). Here the model reflects the peneplanation of the Appalachians and crustal deformation is shown to be the primary cause of the observed positive/negative anomaly couple.

Line 1 is located between the maximum negative and positive values of the gravity profile, proximal to the proposed suture zone in the crustal model. Therefore, mylonite zones parallel to the Taconic suture could extend into the crustal subsurface in the area of the seismic lines. Notice that if the gravity gradient in Figure 13 does indicate the general location of the suture, then the seismic lines get further away from the suture toward the southwest.

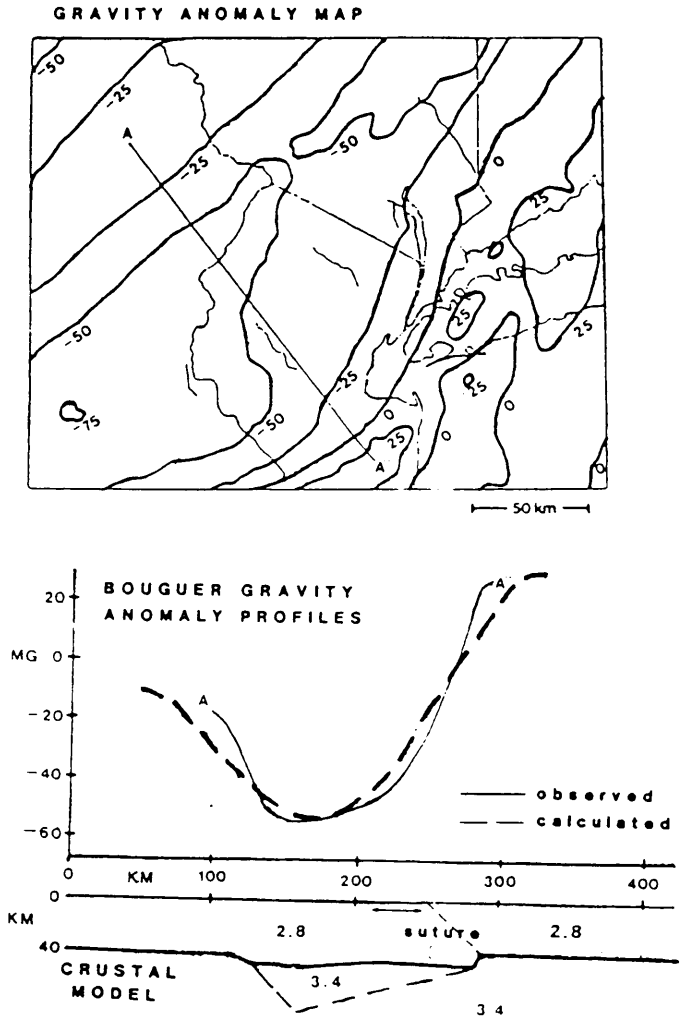

Figure 14. Bouguer gravity anomaly map, observed and calculated gravity profiles, and the crustal model: The model is similar to the Karner and Watts (1982) model (Figure 12) except here the surface is eroded down into the crust. Topographic irregularities are ignored. Observed gravity data from the 1982 SEG gravity map of the U.S. Extent of Line 1 on the model is shown by the arrows.

EARTHQUAKE DATA

Earthquake events in the study area during the period October 1, 1975 to September 30, 1983 have been collected from the Northeastern U.S. Seismic Network Bulletins of Seismicity of the Northeastern U.S. (Nos. 1 to 32). The dates and time of occurrence, latitude and longitude coordinates, depths (km), magnitudes, and ERH/ERZ values for these events are listed in Appendix C. For information concerning the seismic instrumentation, velocity models, and magnitude formulae used in obtaining these data see Kafka (1983) and Ossman (unpubl.). The earthquake epicenters have been plotted along with the seismic reflection lines and the steep gradient in the Appalachian gravity anomaly (Figure 15). Hypocenters were projected onto the vertical seismic sections along geologic strike (Appendix D), which is approximately perpendicular to all the lines except Line 3. Horizontal and vertical error bars defining a 95% confidence of location ellipse have been included where the data were available. For events located halfway between two lines, their hypocenters were projected onto both lines. Several earthquakes also were plotted onto both Lines 25 and 3 because they could be projected onto both lines. No epicenters are located near Line 7 which is farthest from the Taconic suture.

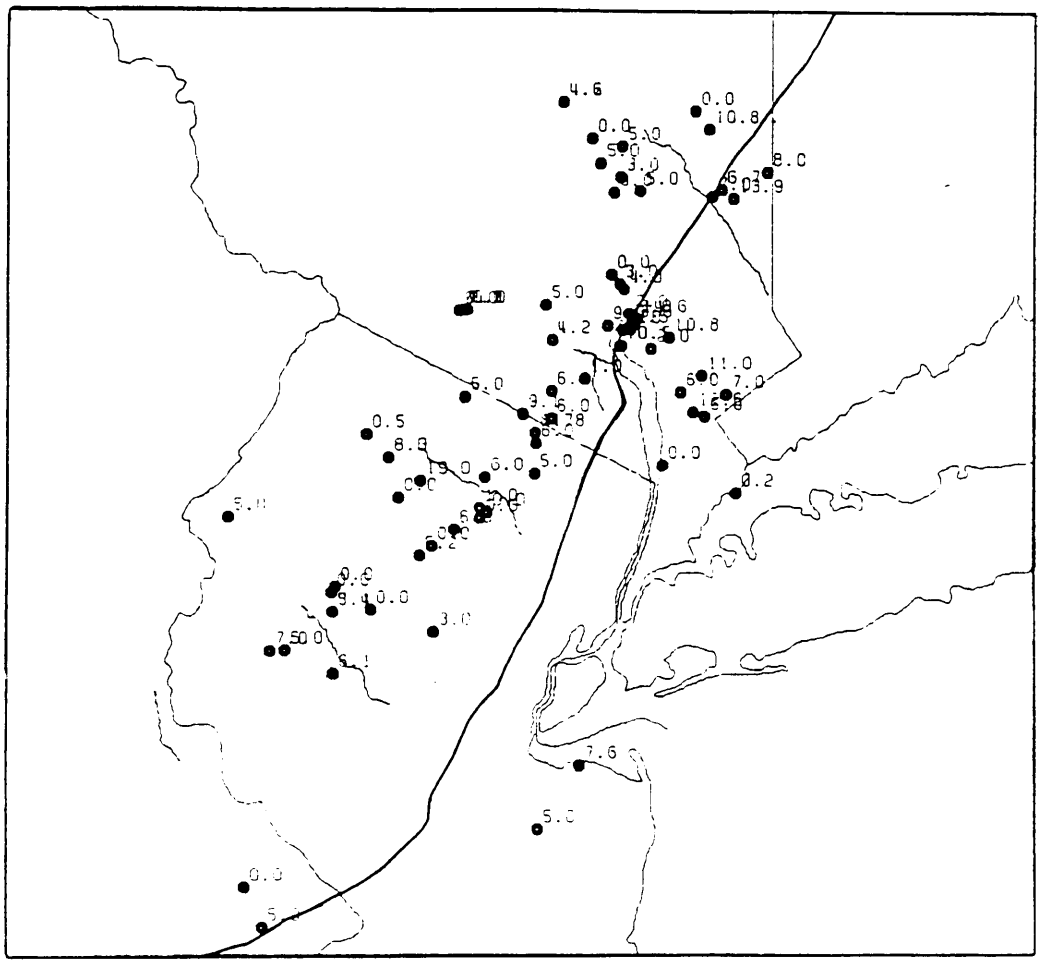

Figure 15. Seismic lines, Bouguer gravity gradient, and earthquake epicenters: Epicenters are indicated by solid circles and focal depths are given in km.

In general, the seismic activity is located within the crystalline basement on the seismic sections. Few earthquakes have locations within the Triassic basins or along the border faults. In addition, there is a volumetric correlation of the mylonite(?) reflections with the earthquake hypocenters. This relationship is apparent to some extent on all of the seismic lines.

For example, on Line 1 several hypocenters occur within reflections interpreted to be from mylonite zones and other hypocenters are located in-line with other possible mylonite zone reflections (Figure 16). Line 25 (Figure 17) contains a similar correspondence of mylonite reflections and earthquake hypocenters. Line 4, located largely over crystalline rocks, has few reflections. However the few deep relatively strong reflections that are observed do have an association with earthquake hypocenters projected onto the section (Figure 17). This apparent correlation of earthquake hypocenters with reflections interpreted to be from mylonite zones may imply that regional stresses are initiating brittle fracture along zones of crustal weakness associated with ancient ductile deformation zones.

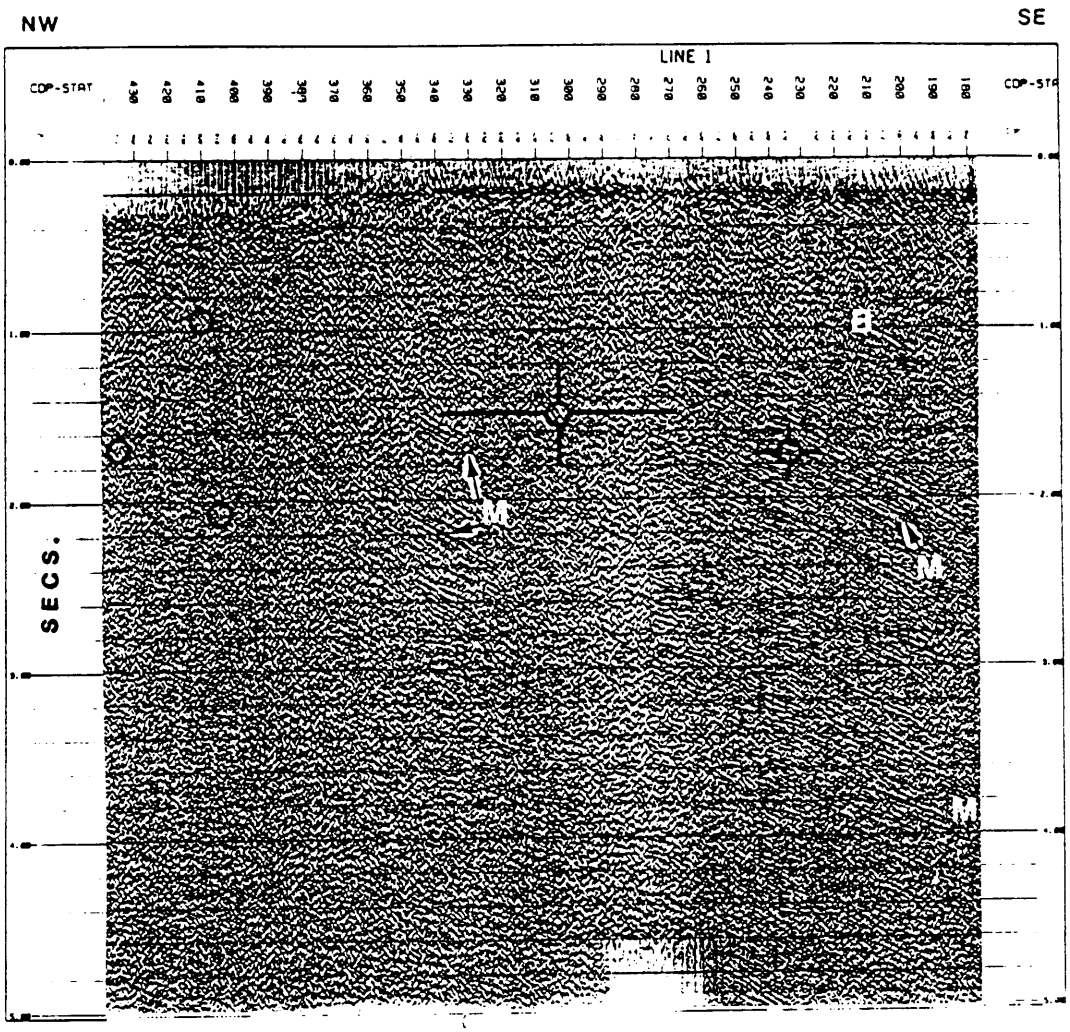

Figure 16. Hypocenters associated with mylonite reflections on Line 1: Part of Line 1 with reflections interpreted to be from mylonite zones labeled 'M' and hypocenters plotted as open circles with ERH/ERZ bars included. Reflection 'B' is from the border fault. (Unmigrated and no vertical exaggeration)

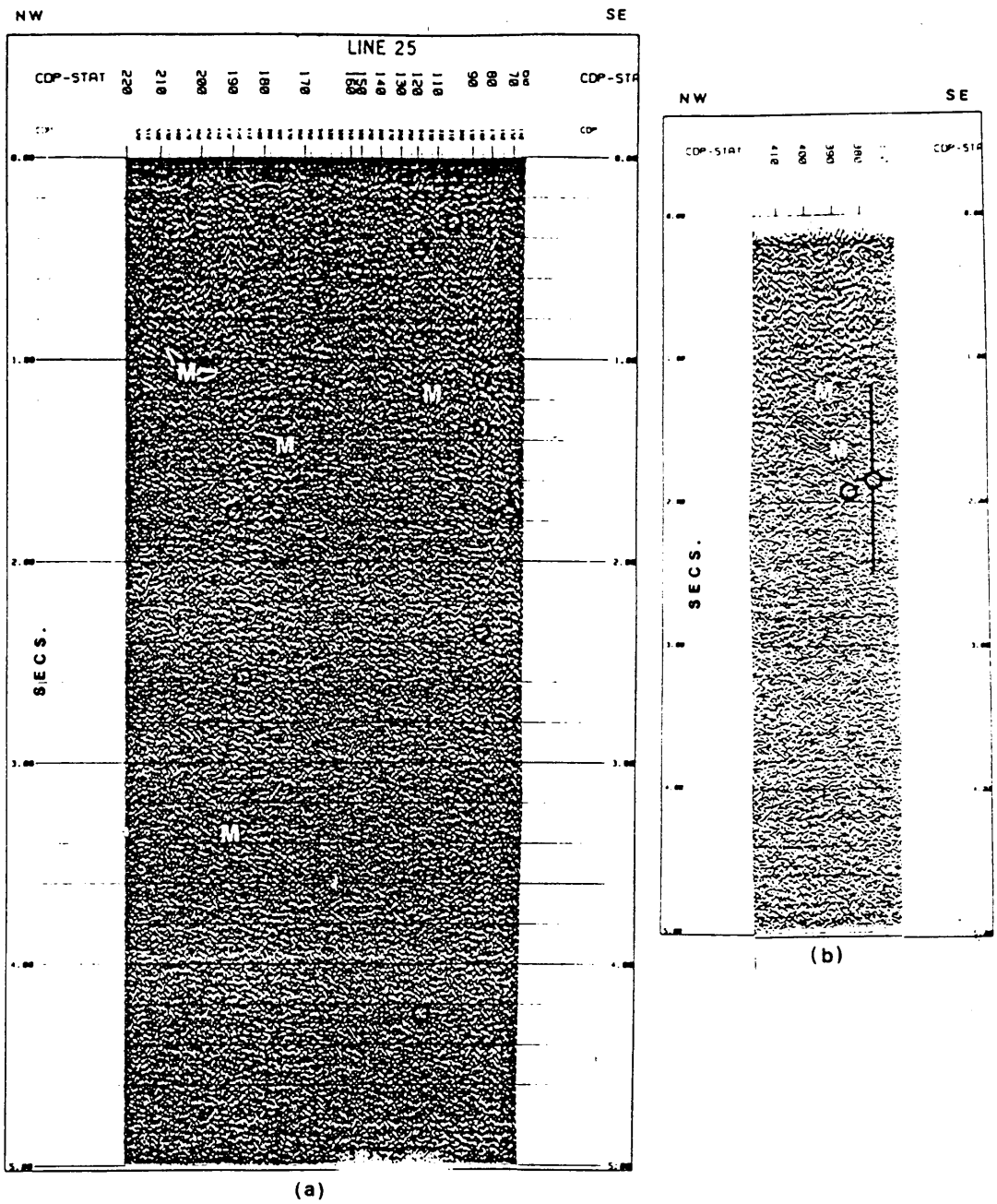

Figure 17. Hypocenters associated with mylonite reflections on Lines 25 and 4: Parts of Line 25 (a) and Line 4 (b) with reflections interpreted to be from mylonite zones labeled 'M' and hypocenters plotted as open circles with ERH/ERZ bars included. (Unmigrated and no vertical exaggeration)

CONCLUSIONS

Reflection seismic data have been processed using various orientations of the common-depth-point sorting line. The vertical sections produced afforded different perspectives of the geology. Generally, the resultant sections were only slightly modified from one another, perhaps due to the fact that almost all of the survey lines were oriented approximately perpendicular to strike.

In the case of Line 3, which was not aligned perpendicular to strike, significant variations in the final section were produced by altering the orientation of the CDP line. Therefore, in certain situations the use of different CDP lines during sorting can be an important method to increase the geologic information in the data.

Residual statics corrections have been demonstrated to considerably enhance the coherency of seismic reflections. These calculations normally require a high signal-to-noise ratio in the data, however even with the relatively low signal-to-noise ratio, the reflection coherency was improved by using an iterative approach to the residual statics corrections. After calculating and applying static corrections the stacking velocity function was reevaluated and residual statics corrections were recalculated. This process was repeated until a maximum level of reflection coherency was

achieved. Often the results included reflections only barely discernible, if at all, in the original data and greatly enhanced the seismic sections and therefore the interpretation of the geologic structure.

Single-sweep processing proved to be a valuable procedure for increasing the geological detail of the seismic data. In particular, local reflections which extend over only a few CDP traces on the original section and thus go unnoticed, become extended over many more CDP traces on the single-sweep section. The results from Line 3 exemplify this effect where small near vertical faults in the basin floor, not apparent on the standard section, became evident on the single-sweep section.

Even when new geologic detail is not produced, the overall coherency and signal-to-noise ratio is improved by single-sweep processing. For example, reflections on the summed single-sweep data appear more laterally continuous than on the standard section. Additionally, the signal-to-noise ratio is noticeably higher even when new geologic information is lacking. Evidently, it is beneficial to apply all steps of the processing routine to each sweep individually and then sum, rather than sum sweeps in the field before processing.

Whether or not single-sweep processing is appropriate and cost-efficient as a standard procedure depends largely upon the specific purposes of the reflection seismic survey

and the degree of geologic complexity encountered. If large volumes of data are involved, for example in petroleum industry exploration, the value of single-sweep processing may not outweigh its expense and time requirements. However, for smaller academic surveys in which the volume of data is less and the geology is more complex, such as in tectonic regimes, single-sweep processing could prove to be worth the time and effort.

Reflection coefficient values calculated from determinations of rock velocities under pressure and modeling of gravity data have provided supporting evidence for reflections originating from mylonite zones. For waves traveling perpendicular to the mineral foliation in the anisotropic mylonites, the contrast in the acoustic impedance between the mylonites and the adjacent isotropic basement granite is enough to generate a detectable p-wave reflection. Deep reflections from within the crystalline basement on the Ramapo lines are interpreted to originate from interfaces between mylonitic and granitic rocks. Furthermore, the mylonites indicate areas of ancient ductile deformation in the crust which now may be zones of crustal weakness.

Earthquake hypocenters projected along geologic strike onto the reflection seismic sections have a distinct association with the mylonite reflections. This relationship seems especially significant because the earthquake hypocenters generally lack any correlation with the Triassic basins or

the brittle border faults. Furthermore, Fischer (1981) stated that movement on the Ramapo fault ceased during Middle to Upper Cretaceous time and Ratcliffe (1980) found no evidence for recent movement in cores taken across the fault. Therefore, it is proposed that stresses in the region may be relieved by brittle fracture along ancient zones of ductile deformation which now are weak zones in the crust marked by mylonitic rocks. Ratcliffe (1980) similarly suggested that current seismic activity may be more strongly controlled by deeply-buried ductile deformation zones than by brittle surface fractures.

During laboratory determinations of velocity, the mylonite rock samples were found to have planes of weakness parallel to the mineral foliation along which the rock samples fractured under relatively low pressures. Perhaps stresses in the earth oriented parallel to these planes of mineral foliation similarly could initiate brittle fracture along the mylonite zones generating the low magnitude earthquakes common in the study area. This theory requires a horizontal compressive stress (σ_1) generally greater than lithostatic stress because,

$$\sigma_1=[\nu/(1-\nu)]\sigma_2 \ ,$$

for a gravity-loaded model, where ν is Poisson's ratio and σ_2 is lithostatic stress.

FUTURE WORK: Ongoing research concerning the occurrence of seismicity in the northeastern U.S. should include the continued integration of geologic, seismic reflection, earthquake, and potential field data. Reflection seismic data coverage could be extended to the east over the location of the Taconic suture with additional lines in other locations along the Ramapo fault zone. Earthquake data could be improved upon by increasing the density of seismic monitoring stations to obtain more confident epicentral and hypocentral locations. At present, accurate focal depth determination is only possible when at least one station is located close enough to the event that the epicentral distance is less than about twice the depth of the event (Kafka, 1983). Detailed analysis of focal mechanism solutions may lead to a better understanding of the orientation and sources of the stress field in the region.

REFERENCES

Aggarwal, Y.P., and Sykes, L.R., 1978, Earthquakes, faults, and nuclear power plants in southern New York and northern New Jersey: Science, no. 200, p. 425.

Airy, G.B., 1855, On the computation of the effect of the attraction of mountain masses as disturbing the apparent astronomical latitude of stations of geodetic surveys: Philos. Trans. R. Soc. London, v. 145, p. 101-104.

Anderson, J. and Dorman, J., 1973, Local geological effects on short-period Rayleigh waves around New York City: Bull. Seis. Soc. Amer., v. 63, p. 1487-1497.

Belcher, S.W., 1984, Spatial resolution by single sweep recording and processing: Masters Thesis, Virginia Polytechnic Institute and State University.

Brooks, M., 1970, Positive Bouguer anomalies in some orogenic belts: Geol. Mag., v. 111, p. 399-400.

Coruh, C. and Costain, J.K., 1983, Noise attenuation by VIBROSEIS whitening (VSW) processing: Geophysics, v. 48 p. 543-554.

Dames and Moore, 1977, Geotechnical investigation of the Ramapo fault system in the region of the Indian Point generating station, Appendix D: Geophysical investigations : report to Consolidated Edison of New York, Inc., v. 1, Cranford, New Jersey.

Dorman, J. and Ewing, M., 1962, Numerical inversion of seismic surface wave dispersion data and crust-mantle structure in the New York-Pennsylvania area, Jour. Geophys. Res., v. 67, p. 5227-5241.

Epstein, J.B., D'Agostino, J.P., Drake, A.A.Jr., and Lampiris, N., 1967, Preliminary log of drill hole near Riegesville, Pennsylvania: Bureau of Topographic and Geologic Survey, Dept. of Internal Affairs, Harrisburg, Pa., 17120.

Fischer, J.A., 1981, Capability of the Ramapo fault system, in Earthquakes and earthquake engineering: the eastern United States, v. 1, J.E. Beavers, editor, Ann Arbor Science, Inc.

Fountain, D.M., Hurich, C.A., and Smithson, S.B., 1984, Seismic reflectivity of mylonite zones in the crust: Geology, v. 12, p. 195-198.

Fountain, D.M., and Salisbury, M.H., 1981, Exposed cross-sections through the continental crust: Implications for crustal structure, petrology and evolution: Earth Planet. Sci. Lett., v. 56, p. 263-277.

Gibb, R.A., and Thomas, M.D., 1976, Gravity signature of fossil plate boundaries in the Canadian Shield: Nature, v. 262, p. 199-200.

Griscom, A., 1963, Tectonic significance of the Bouguer gravity field of the Appalachian system: abstract, Geo. Soc. Amer. Spec. Papers, v. 73, p. 163-164.

Harwood, D.S., and Zietz, I., 1974, Configuration of Precambrian rocks in southeastern New York and adjacent New England from aeromagnetic data: Geol. Soc. Amer. Bull., v. 85, p. 181-188.

James, D.E., Smith, T.J., and Steinhart, J.S., 1968, Crustal structure of the middle Atlantic states, Jour. Geophys. Res., v. 73, p. 1983-2008.

Jones, T.D., and Nur, A., 1984, The nature of seismic reflections from deep crustal fault zones: J. Geophys. Res., v. 89, p. 3153-3171.

Kafka, A.L., 1983, Earthquake hazard studies in New York State and adjacent areas: Final Report, April 1976-June 1982, Lamont-Doherty Geological Observatory report to U.S. Nuclear Regulatory Commission.

Kafka, A.L., Schlesinger-Miller, E.A., Barstow, N.L., Cramp, D., and Sykes, L.R., 1982, Earthquake magnitudes and seismicity in the New York City metropolitan area: Preprint (To be submitted for publication to BSSA).

Karner, G.D., and Watts, A.B., 1983, Gravity anomalies and flexure of the lithosphere at mountain ranges: J. Geophys. Res., v. 88, p. 10449-10477

Karner, G.D., and Watts, A.B., 1982, On isostasy at Atlantic-type continental margins: J. Geophys. Res., v. 87, p. 2923-2948.

Karner, G.D., 1981, Global data bank system: Tech. Rep. 1, CU-1-81, v. 27, Lamont-Doherty Geol. Observ. of Columbia Univ., Palisades, N.Y.

Klemperer, S.L., and Brown, L., 1985, Simulations of noise rejection and mantissa-only recording: An experiment in high-amplitude noise reduction with COCORP data: Geophysics, v. 50, p. 709-714.

Levin, F.K., 1971, Apparent velocity from dipping interface reflections: Geophysics, v. 36, p. 510-516.

Neidell, N.S., 1984, Stratigraphic modeling and interpretation: Geophysical principles and techniques: Amer. Assoc. Petrol. Geol. Education Course Note Series #13.

Nuttli, O.W., 1973, Seismic wave attenuation and magnitude relations for eastern North America: J. Geophys. Res., v. 78, p. 876-885.

Osberg, P.H., 1978, Synthesis of the geology of the northeastern Appalachians, U.S.A., IGCP Project 27: Geol. Surv. Canada, Paper 78-13, 1377-147.

Ossman, R.M., 1984, Seismotectonics of southeastern New York State, Masters Thesis, The Pennsylvania State University.

Page, R.A., Molnar, P.H., and Oliver, J., 1968, Seismicity in the vicinity of the Ramapo fault, New-Jersey-New York: Bull. Seis. Soc. Amer., v. 58, no. 2, p. 681-687.

Pratt, J.H., 1855, On the attraction of the Himalayan Mountains, and of the elevated regions beyond them, upon the plumb line in India: Philos. Trans. R. Soc., v. 145, p. 53-100.

Ratcliffe, N.M., 1968, Contact relations of the Cortlandt Complex at Stony Point, New York, and their regional implications: Geol. Soc. Amer. Bull., v. 79, p. 777-786.

Ratcliffe, N.M., and Shuart, S.G., 1970, The Rosetown complex and its bearing on the antiquity of the Ramapo fault system: Geol. Soc. Amer. Abstr., part 1, (northeast. sect.), p. 32-33.

Ratcliffe, N.M., 1971, The Ramapo fault system in New York and adjacent New Jersey: a case of tectonic heredity: Geol. Soc. Amer. Bull., v. 82, p. 125-141.

Ratcliffe, N.M., 1976, Final report on major fault systems in the vicinity of Tompkins Cove-Buchanan, New York: report for Woodward-Clyde Consultants, Wayne, New Jersey.

Ratcliffe, N.M., 1980, Brittle faults (Ramapo fault) and phyllonitic ductile shear zones in the basement rocks of the Ramapo seismic zone, New York and New Jersey, and their relationship to current seismicity: in Field studies of New Jersey geology and guide to field trips, Rutgers University, Newark, New Jersey.

Ratcliffe, N.M., 1982, Fault reactivation and seismicity in the Ramapo seismic zone, New York-New Jersey: Abstr.-Eqke. Notes, v. 53, p. 32. Sbar, M.L., Rynn, J.M.W., Gumper, F.J., and Lahr, J.C., 1970, An earthquake sequence and focal mechanism solution, Lake Hopatcong, northern New Jersey: Bull. Seis. Soc. Amer., v. 60, p. 1231-1243.

Sbar, M.L., and Sykes, L.R., 1973, Contemporary compressive stress and seismicity in eastern North America: an example of intra-plate tectonics: Geol. Soc. Amer. Bull., v. 84, p. 1861-1882.

Sbar, M.L., Aggarwal, Y.P., and Sykes, L., 1976, Study of earthquake hazards in New York and adjacent states, phase III annual technical report, for New York State Development Authority and United States Nuclear Regulatory Commission: Lamont-Doherty Geological Observatory, Palisades, New York.

Sbar, M.L., 1975, In-situ stress measurement program, field results. Determination of the regional stress field in New York State and adjacent areas by in-situ strain relief measurements: for New York State Energy Research and Development Authority, New York, New York. (NTIS)

Sbar, M.L., Rynn, J.M.W., Gumper, F.J., and Lahr, J.C., 1970, An earthquake sequence and focal mechanism solution, Lake Hopatcong, northern New Jersey: Bull. Seismol. Soc. Amer., v. 60, p. 1231-1243.

Simpson, R.W., Bothner, W.A., and Godson, R.H., 1981, Colored gravity anomaly and terrain maps of the northeastern U.S. and adjacent Canada: U.S. Geol. Surv. Open File Rept. 81-560.

Sykes, L.R., 1978, Intraplate seismicity, reactivation of preexisting zones of weakness, alkaline magmatism, and other tectonism postdating continental fragmentation: Rev. Geophys. and Space Physics, v. 16, p. 621-688.

Tanner, J.G., 1969, A geophysical interpretation of structural boundaries in the eastern Canadian Shield, Ph.D. thesis, Univ. of Durham, Durham, United Kingdom.

Telford, W.M., Geldart, L.P., Sheriff, R.E., and Keys, D.A., 1976, Applied Geophysics: Cambridge University Press.

Turcotte, D.L., and Schubert, G., 1982, Geodynamics, Applications of Continuum Physics to Geological Problems: John Wiley, New York.

Watts, A.B., Karner, G.D., and Steckler, M.S., 1982, Lithospheric flexure and the evolution of sedimentary basins: Philos. Trans. R. Soc. London, Ser. A, v. 305, p. 249-281.

Watts, A.B., 1981, The U.S. Atlantic continental margin: Subsidence history, crustal structure and thermal evolution: in Geology of Passive Continental Margins: History, Structure, and Sedimentologic Record, Educ. Course Note Ser., v. 19, Amer. Assoc. Petr. Geol., Tulsa, Okla.

Yang, J.P., and Aggarwal, Y.P., 1981, Seismotectonics of northeastern United States and adjacent Canada: J. Geophys. Res., v. 86, p. 4981-4988.

Zietz, I., King, E.R., Geddes, W., and Lidich, E.G., 1966, Crustal study of a continental strip from the Atlantic Ocean to the Rocky Mountains: Geol. Soc. Amer. Bull., v. 77, p. 1427-1448.

Zoback, M.L., and Zoback, M., 1980, State of stress in the conterminous United States: J. Geophys. Res., v. 85, p. 6113-6156.

APPENDIX A. LOCATIONS OF RAMAPO LINES

RAMAPO LINE1 was acquired from 9/5/83 to 9/8/83 in Somerville, New Jersey along state route 517 (Bound Brook, Raritan, Gladstone, Califon, and Hackettstown USGS 7.5' quadrangles).

RAMAPO LINE2 was acquired from 9/9/83 to 9/10/83 in Rockland County, New York, near the city of Stoney Point along state route 210 (Haverstraw, Thiells, and Popolopen Lake USGS 7.5' quadrangles).

RAMAPO LINE3 was acquired from 9/11/83 to 9/12/83 also near the city of Stoney Point, New York, along the Palisades Interstate Parkway (Thiells and Popolopen Lake USGS 7.5' quadrangles).

RAMAPO LINE4 was acquired from 10/25/83 to 11/4/83 starting near the New York/Connecticut state border going Northwest along routes 121 and 6, Interstate 84, Storm Mountain Road, routes 52 and Old 52, route 216, Phillips Road, Sylvan Lake Road and Old Sylvan Lake Road, Arthursburg Road, and Noxon Road (Peach Lake, Brewster, Lake Carmel, Poughquag, Hopewell Junction, and Pleasant Valley USGS 7.5' quadrangles).

RAMAPO LINE5 was acquired from 11/5/83 to 11/6/83 also near Stoney Point, New York, along route 210 overlapping part of RAMAPO LINE2 (Haverstraw and Thiells USGS 7.5' quadrangles).

RAMAPO LINE6 was acquired from 11/8/84 to 11/13/84 in Passaic County, New Jersey, near the city of Patterson along state route 23 (Franklin, Newfoundland, Pompton Plains, and Wanaque USGS 7.5' quadrangles).

RAMAPO LINE7 was acquired from 11/14/84 to 11/18/84 near Bethlehem and Riegelsville, Pennsylvania along state route 412, Gallows Hill Road, route 212, Durham Road, and Raubville Road (Bedminster, Riegelsville, and Easton USGS 7.5' quadrangles).

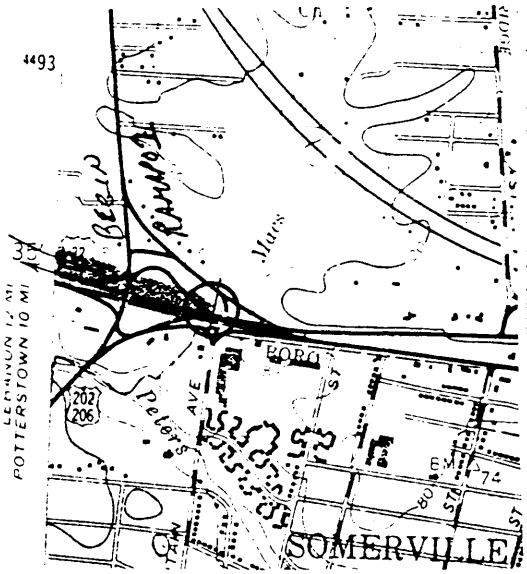

Begin Line 1
Bound Brook Quad

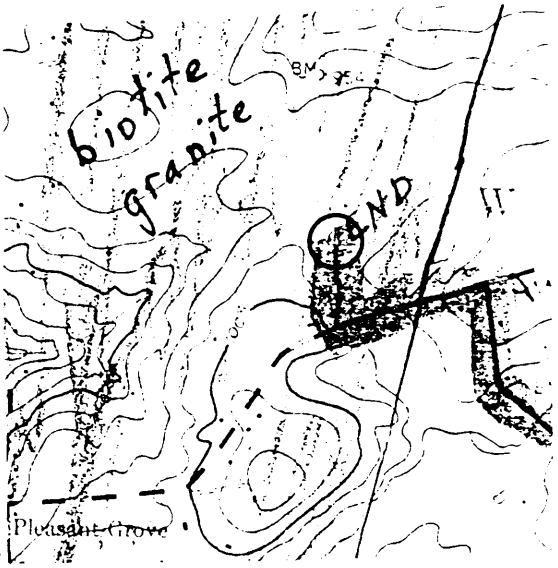

End Line 1
Hackettstown Quad

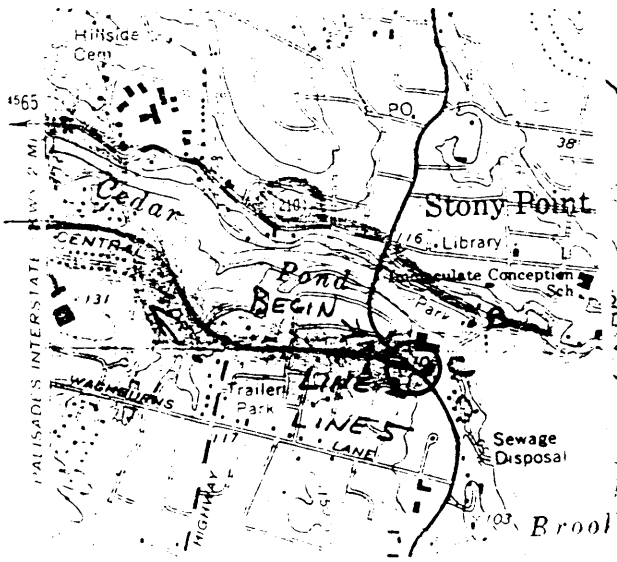

Begin Line 25
Haverstraw Quad

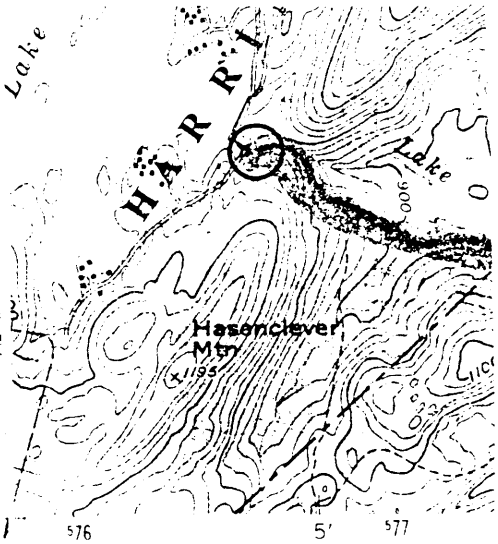

End Line 25
Popolopen Quad

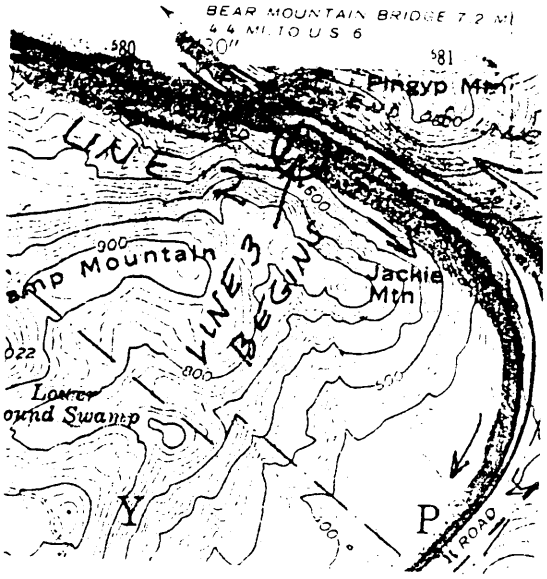

Begin Line 3
Thiells Quad

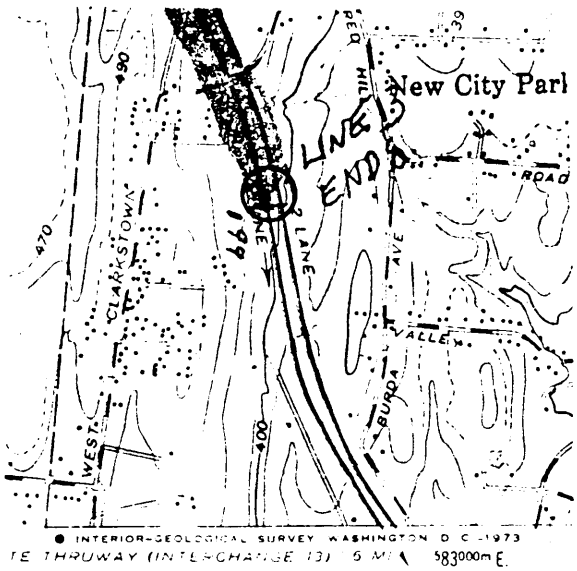

End Line 3
Thiells Quad

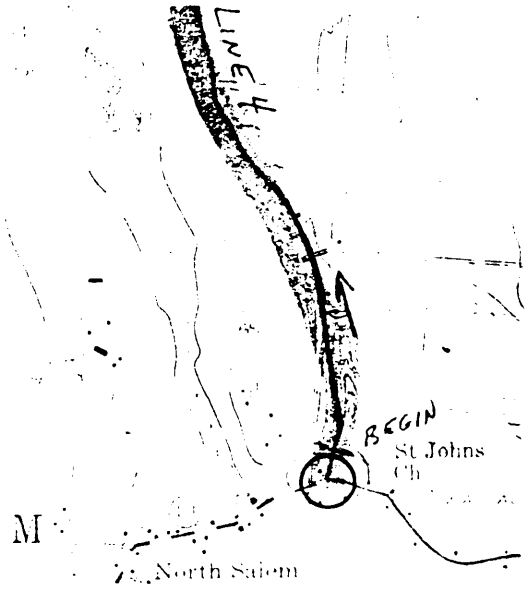

Begin Line 4
Peach Lake Quad

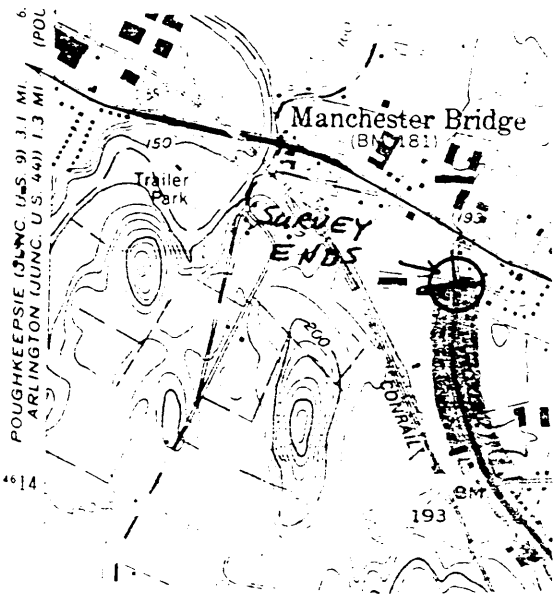

End Line 4
Pleasant Valley Quad

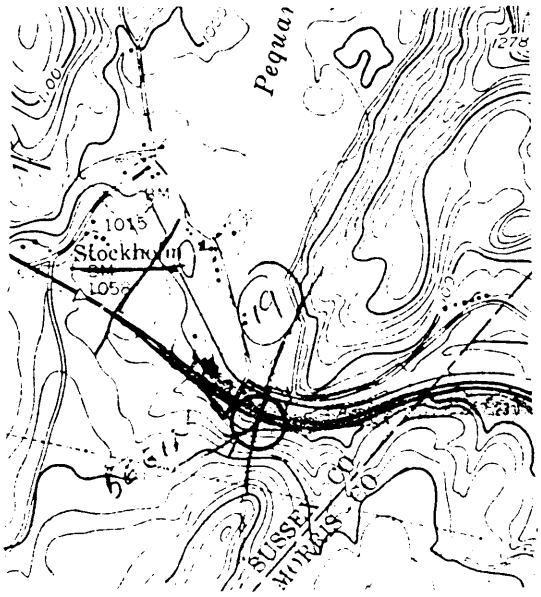

Begin Line 6
Franklin Quad

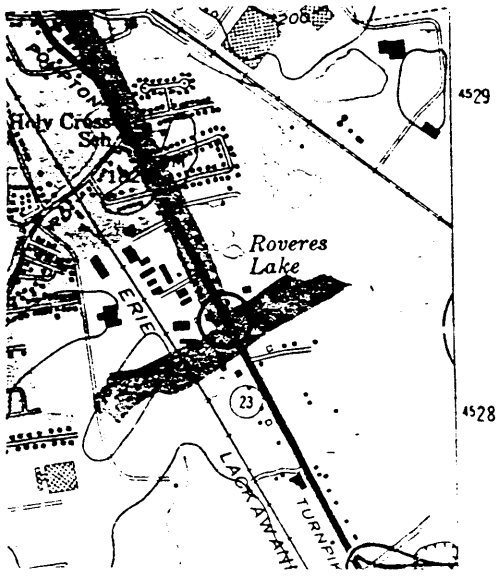

End Line 6
Pompton Plains Quad

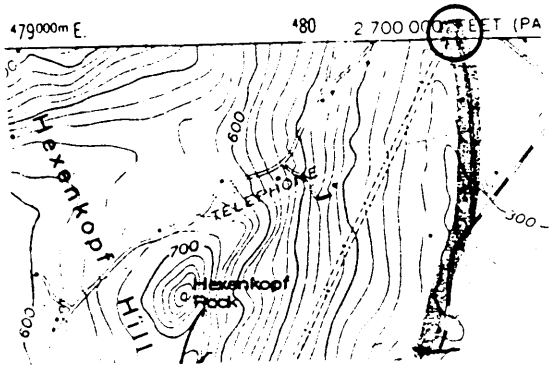

Begin Line 7
Riegelsville Quad

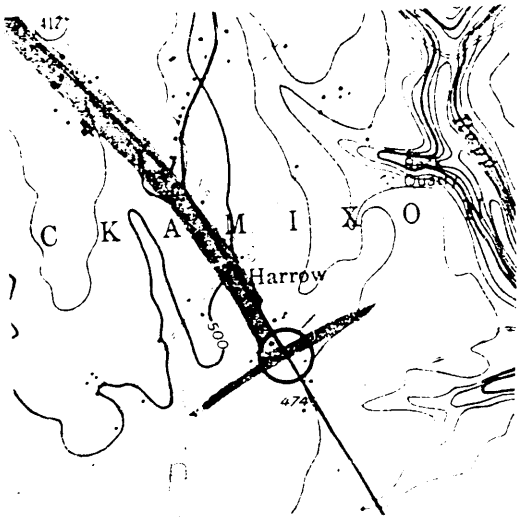

End Line 7
Bedminster Quad

APPENDIX B. STANDARD PROCESSING ROUTINE

Demultiplexing and Correlation

First, normal demultiplexing was performed on the data, followed by a modification to a normal correlation. The unusual correlation technique was the application of VIBROSEIS Whitening (VSW) (Coruh and Costain, 1983). This process involves applying an automatic gain control (AGC) to the data before correlation to balance the spectral content of the record (whiten the data). This process was applied to all the data with an AGC window of 1.0 sec.

Normally the individual sweeps are summed in the field or after correlation. However, for single-sweep processing, the individual sweeps are not summed, but continue through the entire processing sequence as separate shots. This procedure was applied to Lines 1, 2, 3, and 5.

Editing;

Hand-editing of the data consisted of deleting bad shot records and traces with prevalent high or low frequency noise.

Geometry and Datum Statics;

The geometry for each line was defined directly from the survey data and observer's notes.

Datum statics were applied using the average elevation of the line as the datum elevation and the average direct wave velocity as the datum velocity.

CDP Sorting;

CDP sorting was applied to the data often several times using different CDP line orientations.

Velocity Analysis and Mute

A standard velocity analysis was performed on the data using constant velocity stacks (CVAs). On several lines, the velocity analysis was done in an iterative fashion, alternating with the residual statics applications.

Mute functions were applied to the lines to eliminate first breaks, refractions, and wavelet stretching. Experimentations with several different mute patterns were undertaken since many of the lines contained important near surface reflections.

Residual Static Corrections

Datum statics, followed by extensive surface consistent residual statics analyses were applied to the data. The residual statics were computed in an iterative

manner; a velocity function was chosen, residual statics applied, then often another velocity analysis was done and the velocity function revised if necessary. This sequence was repeated several times (usually three or four) on most lines to optimize the statics used for the final sections by accumulating the calculated values after each run.

An unconventional time-variant residual statics calculation also was applied to some of the lines.

Band-Pass Filtering

A band-pass filter of 14 to 56 Hz was applied.

Migration

Post-stack migration also was performed. The single-sweep data were not migrated.

APPENDIX C. EARTHQUAKE EPICENTRAL/HYPOCENTRAL DATA

Yr MoDy	Hr:Mn	Lat(Dg)	Lon(Dg)	Depth	Mag	ERH	ERZ
1983 915	23:17	41.139	-74.230	9.1	1.5	0.7	0.78
1983 913	2:46	41.260	-73.958	10.5	1.4	0.22	0.41
1983 913	3:53	41.260	-73.960	10.1	1.9	0.18	0.32
1983 6 1	9:50	40.872	-74.525	5.2	1.5	1.69	0.96
1983 426	19:36	41.533	-73.635	13.9	1.4	2.0	1.7
1983 4 7	20:34	41.672	-73.687	10.8	1.6	1.7	1.1
1983 226	19:59	41.552	-73.663	6.7	3.0	0.24	2.25
1983 219	5:45	40.648	-74.768	6.1	2.7	0.26	0.52
1983 121	21:21	40.955	-73.682	0.2	2.2	1.14	1.6
1982 916	6:36	41.118	-74.645	0.5	1.6	1.7	31.6
1982 818	4:30	41.127	-74.155	6.0	2.0	0.2	0.1
1982 6 2	3:27	41.745	-74.070	4.6	1.5	0.7	0.3
1981 621	5:04	41.070	-74.590	8.5	1.8		
1981 518	7:22	41.100	-74.200	8.7	2.2		
1981 518	7:22	41.100	-74.200	11.8	2.3		
1981 319	8:51	40.940	-74.360	9.6	1.9		
19801212	23:04	41.310	-73.910	14.6	2.3		
19801212	23:04	41.270	-73.830	10.8	1.7		
19801015	17:02	41.250	-73.880	2.0	1.5		
1980 927	0:48	41.540	-73.690	7.0	2.2		
1980 9 4	4:30	41.120	-73.780	12.6	2.9		
1980 8 2	17:21	40.440	-74.140	7.6	3.0		
1980 520	21:33	41.350	-74.370	2.3	2.6		
1980 512	1:38	41.280	-74.140	4.2	2.4		
1980 5 7	4:32	41.020	-73.870	0.0	2.6		
1980 5 2	19:02	40.240	-75.030	0.0	3.0		
1980 5 2	15:23	40.160	-74.990	5.0	2.8		
1980 425	0:23	41.350	-74.370	0.0	2.4		
1980 325	18:54	40.970	-75.020	5.0	2.8		
1980 117	10:13	41.300	-73.920	3.6	2.8		
1980 117	10:12	41.290	-73.930	4.5	1.9		
19791230	14:50	41.150	-73.690	7.0	2.3		
197912 1	16:14	41.350	-74.360	0.0	1.9		
197910 1	19:50	41.650	-73.920	5.0	0.0		
1979 9 4	7:38	41.580	-73.540	8.0	1.1		
1979 620	19:20	41.350	-74.380	0.0	0.0		
1979 310	4:49	40.720	-74.500	3.0	3.1		
1979 211	7:21	41.190	-73.750	11.0	2.0		
1979 2 2	2:26	40.770	-74.660	0.0	1.9		
1979 130	16:30	40.320	-74.260	5.0	3.5		
1978 723	23:02	41.320	-73.930	2.0	2.1		
1978 630	22:39	41.080	-74.200	6.0	1.8		
1978 630	20:13	41.080	-74.200	5.0	2.7		

1978 616	4:59	40.990	-74.570	0.0	0.0
1978 518	1:29	41.020	-74.340	6.0	1.5
1978 3 5	7:53	41.350	-74.150	5.0	2.1
1978 215	5:28	40.920	-74.430	6.0	1.6
1978 210	9:37	41.300	-73.990	9.0	0.0
1978 115	7:41	41.380	-73.950	3.0	0.0
1978 114	18:47	41.370	-73.940	4.0	0.0
1978 113	5:15	41.400	-73.970	0.0	0.0
19771226	16:54	40.810	-74.760	0.0	1.7
19771225	15:39	40.810	-74.760	0.0	1.5
19771224	10:25	40.810	-74.760	0.0	1.6
19771223	16:20	40.810	-74.760	0.0	1.4
19771223	4:55	40.820	-74.750	0.0	2.2
197712 9	17:33	41.560	-73.880	5.0	2.3
197712 6	8:34	40.810	-74.760	0.0	1.7
197712 6	17:51	40.810	-74.760	0.0	1.6
197712 4	23:50	40.810	-74.760	0.0	2.1
197712 4	23:50	40.810	-74.760	0.0	1.8
19771127	13:57	41.020	-74.210	5.0	1.8
19771027	9:22	41.070	-74.590	6.0	1.5
19771014	9:53	41.560	-73.950	0.0	2.4
1977 917	18:47	41.200	-74.060	1.0	0.0
1977 9 2	5:53	41.310	-73.920	3.0	2.4
1977 7 2	11:13	40.700	-74.930	7.0	2.3
1977 610	12:48	40.700	-74.890	6.0	1.1
1977 310	16:22	41.180	-74.150	6.0	2.2
1977 1 7	0:05	41.020	-74.510	19.0	0.0
197612 7	4:55	40.770	-74.760	5.1	1.7
197612 5	16:32	40.770	-74.760	3.4	1.8
19761028	1:13	40.890	-74.490	0.0	0.7
1976 922	9:04	41.290	-73.950	8.0	1.8
1976 820	22:08	41.110	-73.750	6.0	2.5
1976 312	10:28	40.950	-74.340	0.0	2.2
1976 311	21:07	40.960	-74.360	1.0	2.4
1976 3 6	4:14	41.160	-73.810	6.0	2.3
19751110	3:02	41.180	-74.380	5.0	1.8
197511 2	4:09	41.670	-74.000	0.0	0.0
19751028	21:45	41.710	-73.720	0.0	0.0
19751024	7:43	41.590	-73.930	3.0	2.2
19751024	7:08	41.620	-73.980	5.0	2.0

APPENDIX D. REFLECTION SEISMIC SECTIONS

Unmigrated and migrated reflection seismic lines from the Ramapo fault zone plotted with no vertical exaggeration (one to one scale). Open circles on the unmigrated sections represent earthquake hypocenters. ERH and ERZ bars are included for events with that information. Detailed geologic interpretations of the reflection seismic lines is being undertaken by Nick Ratcliffe of the U.S.G.S., Reston. Here the main reflections on the unmigrated seismic lines are labeled according to the following classifications:

(1) Reflections from sedimentary/basement interfaces, i.e., the Triassic basin bounding faults. Labeled 'B'.

(2) Reflections from intrusive basaltic flows within the sedimentary basins, e.g., the Palisades sill (Line 1). Labeled 'I'.

(3) Reflections from within the crystalline basement which are interpreted to be from mylonite(?) zones. Labeled 'M'.

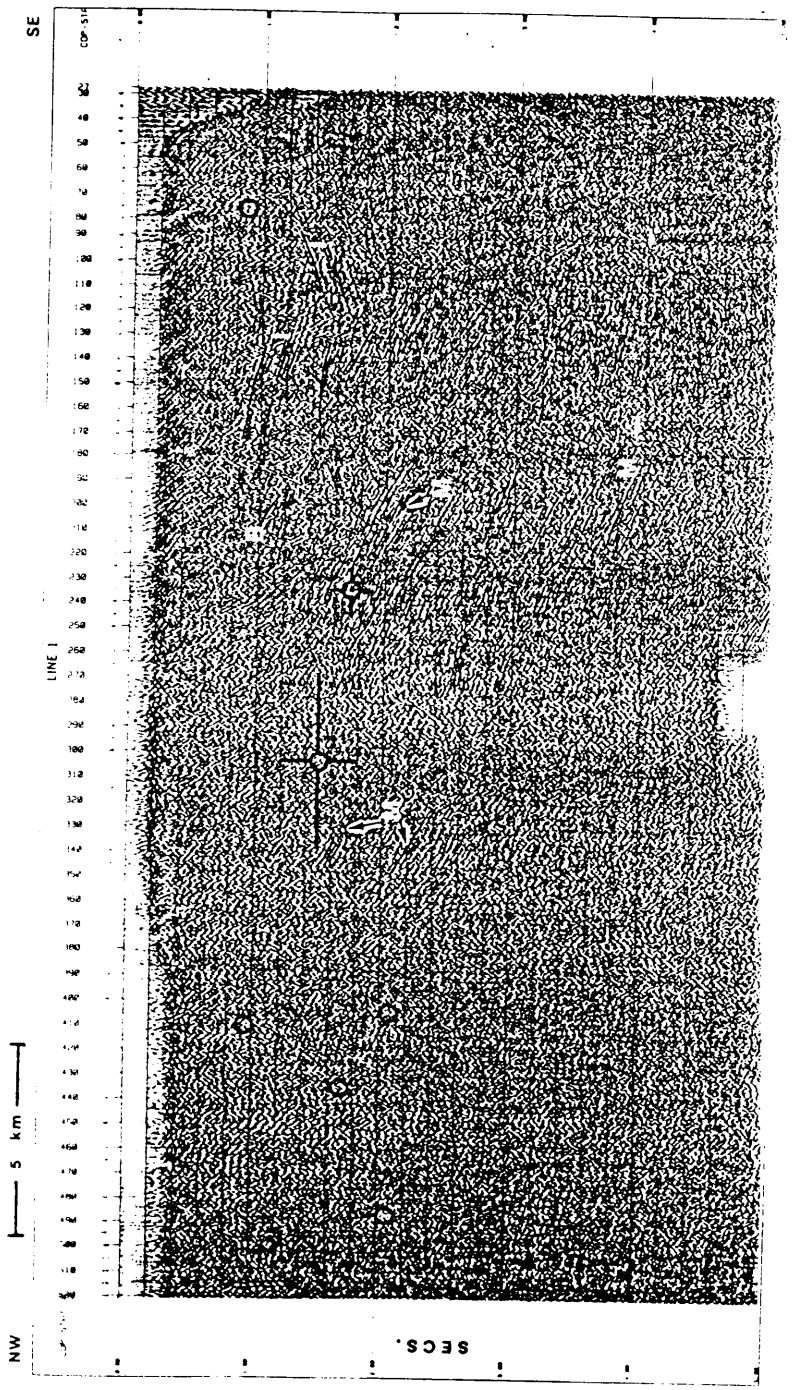
SE
NW
LINE 1
5 km
SECS.

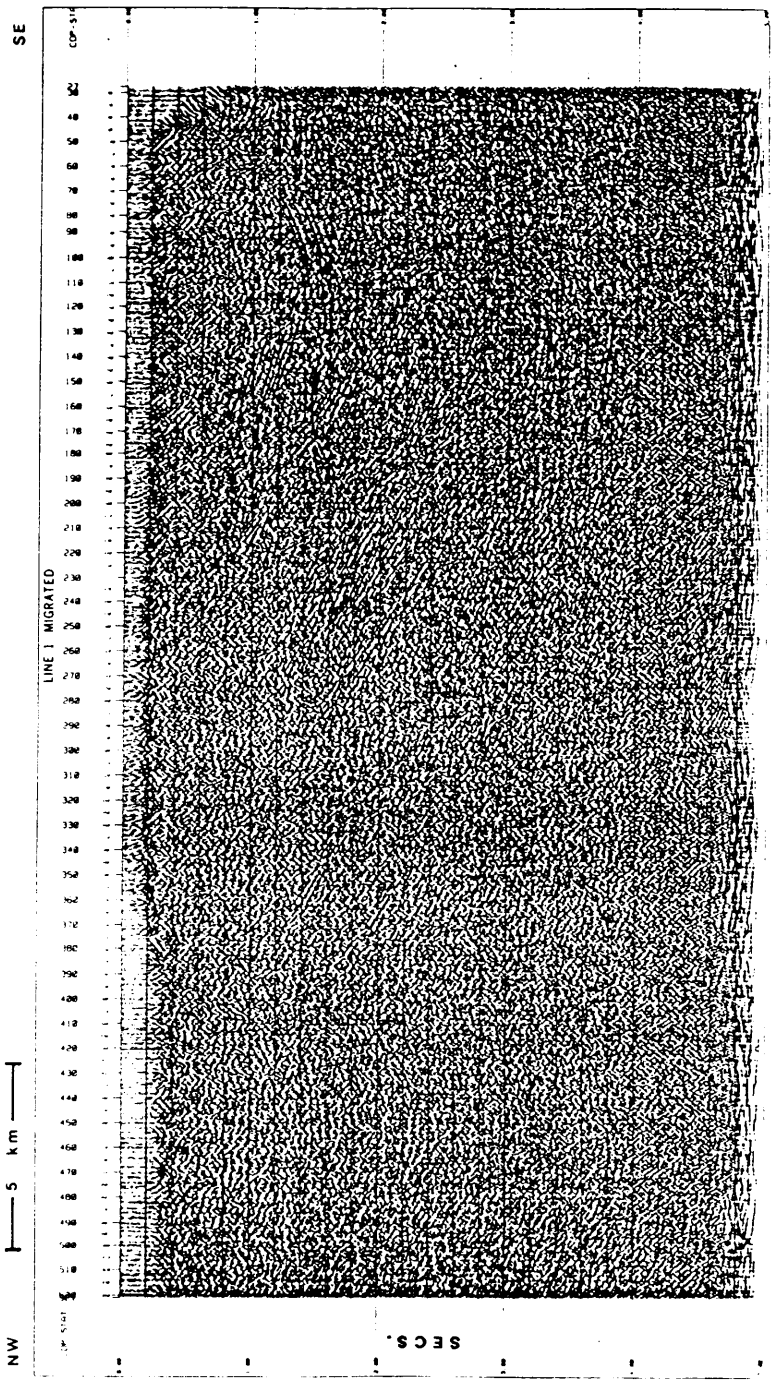
SE
NW
LINE 1 MIGRATED
5 km
SECS.

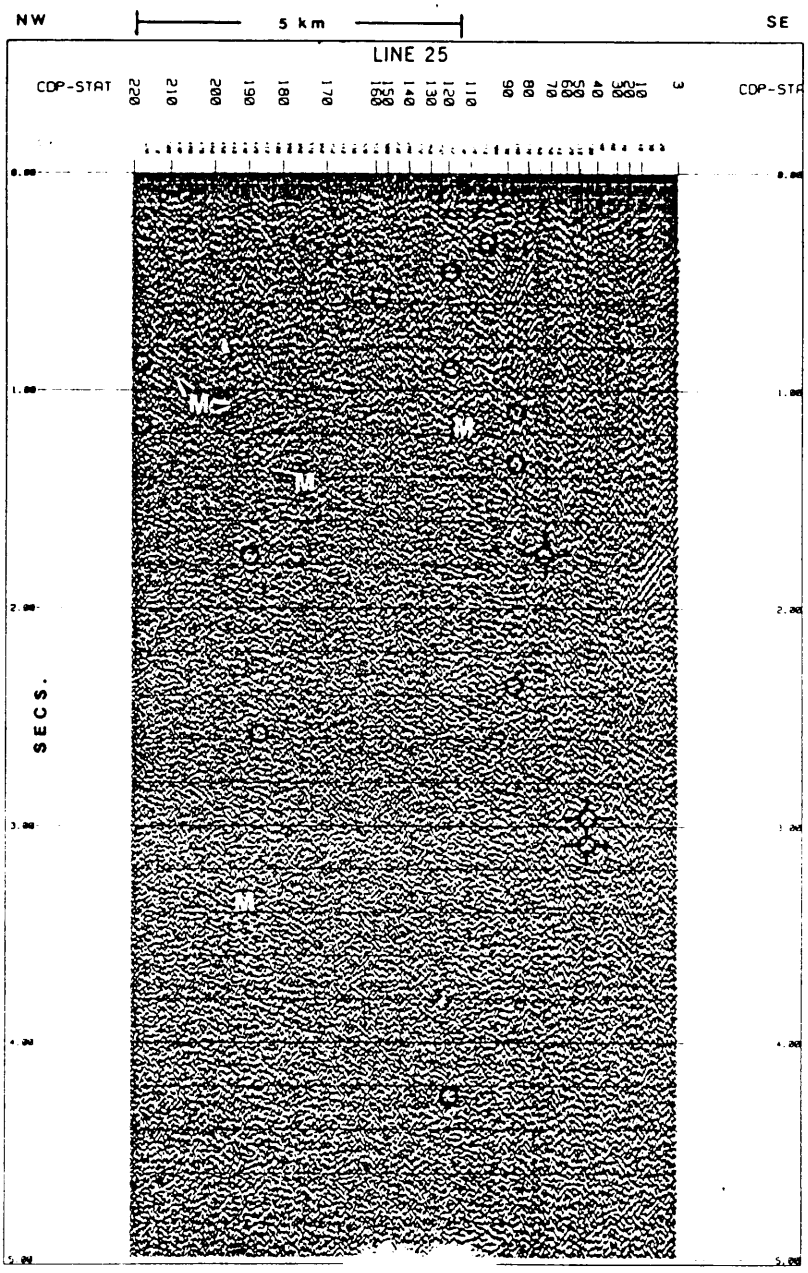
NW
5 km
SE
LINE 25
CDP-STAT
220
210
200
190
180
170
160
150
140
130
120
110
90
80
70
60
50
40
30
20
10
3
CDP-STA
SECS.
M
M
M

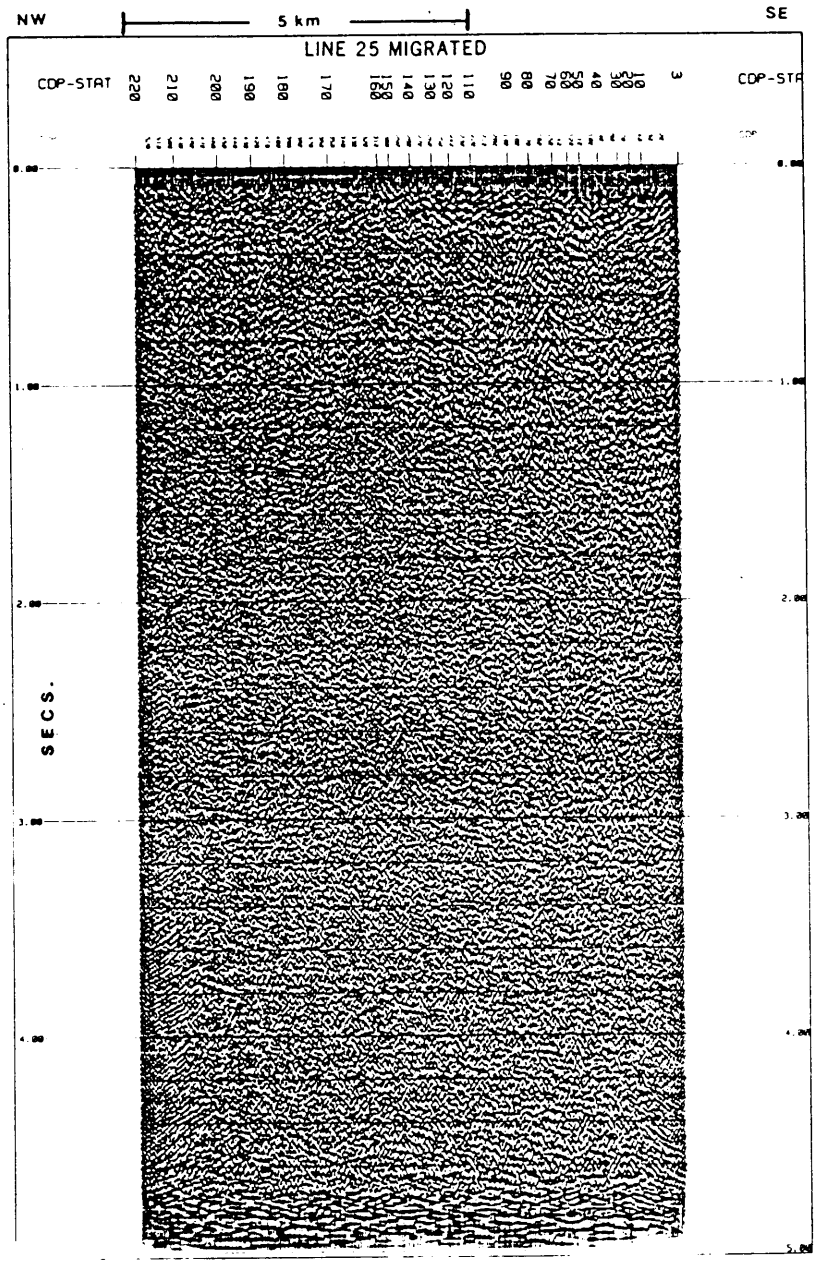
NW
5 km
SE
LINE 25 MIGRATED
CDP-STAT
220
210
200
190
180
170
160
150
140
130
120
110
90
80
70
60
50
40
30
20
10
3
CDP-STA
SECS.

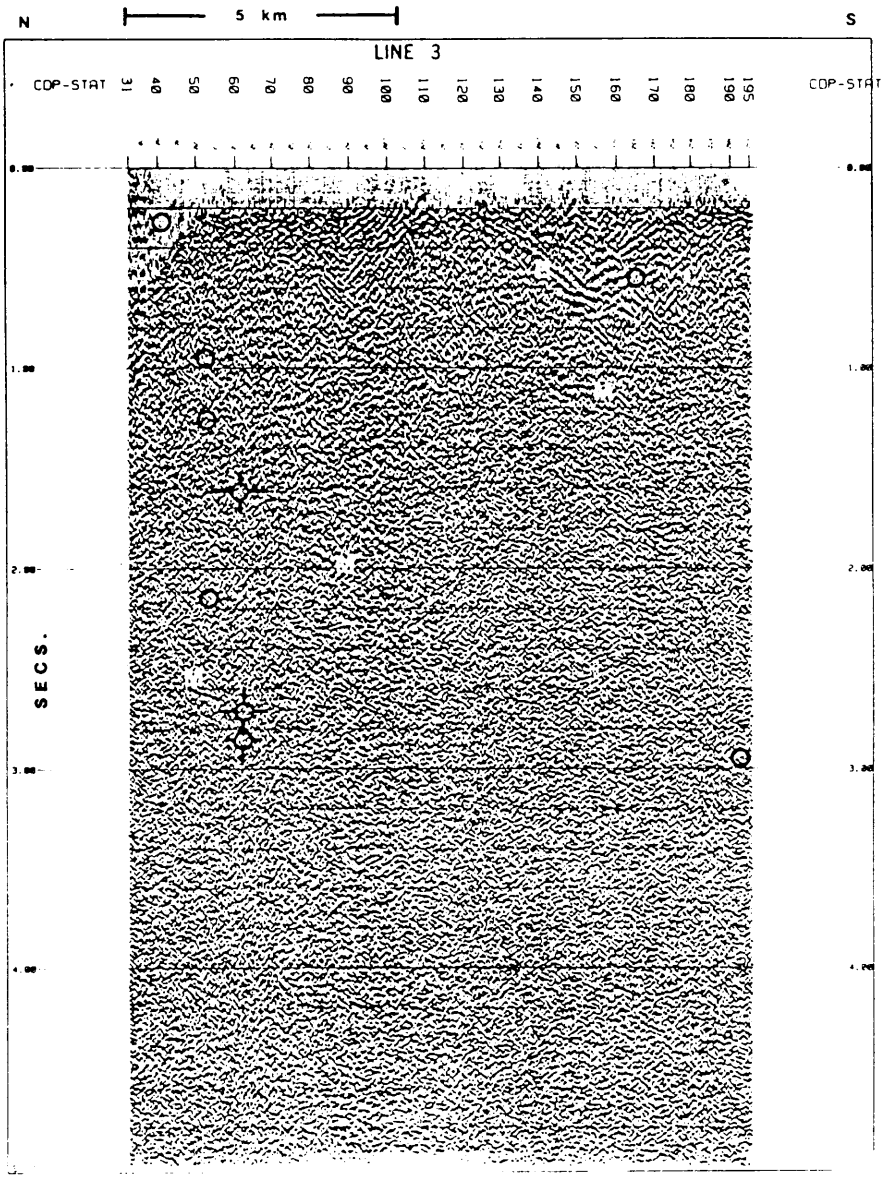
N
5 km
S
LINE 3
COP-STAT
31
40
50
60
70
80
90
100
110
120
130
140
150
160
170
180
190
195
COP-STAT
SECS.

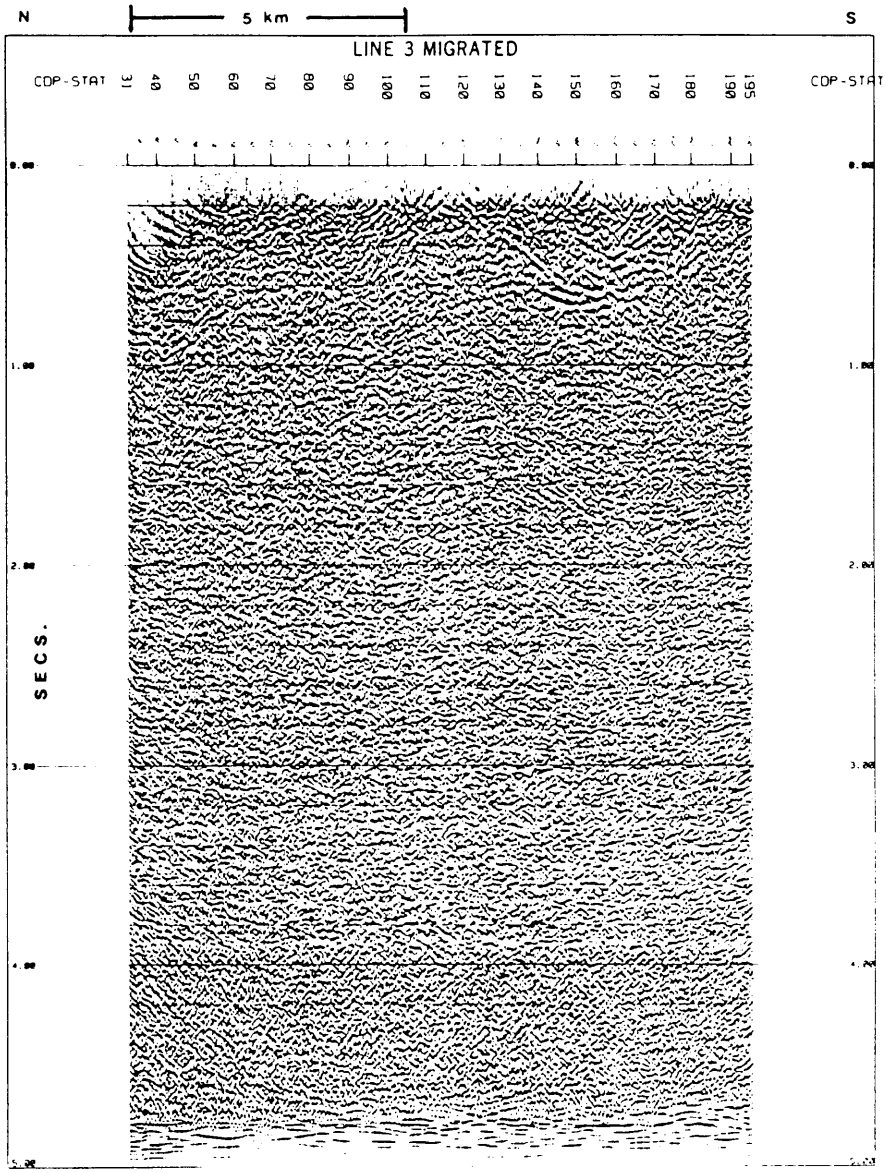
N
5 km
S
LINE 3 MIGRATED
CDP-STAT
31
40
50
60
70
80
90
100
110
120
130
140
150
160
170
180
190
195
CDP-STAT
SECS.

SE
NW
LINE 4
5 km
SECS.

SE
NW
LINE 4
5 km
SECS.

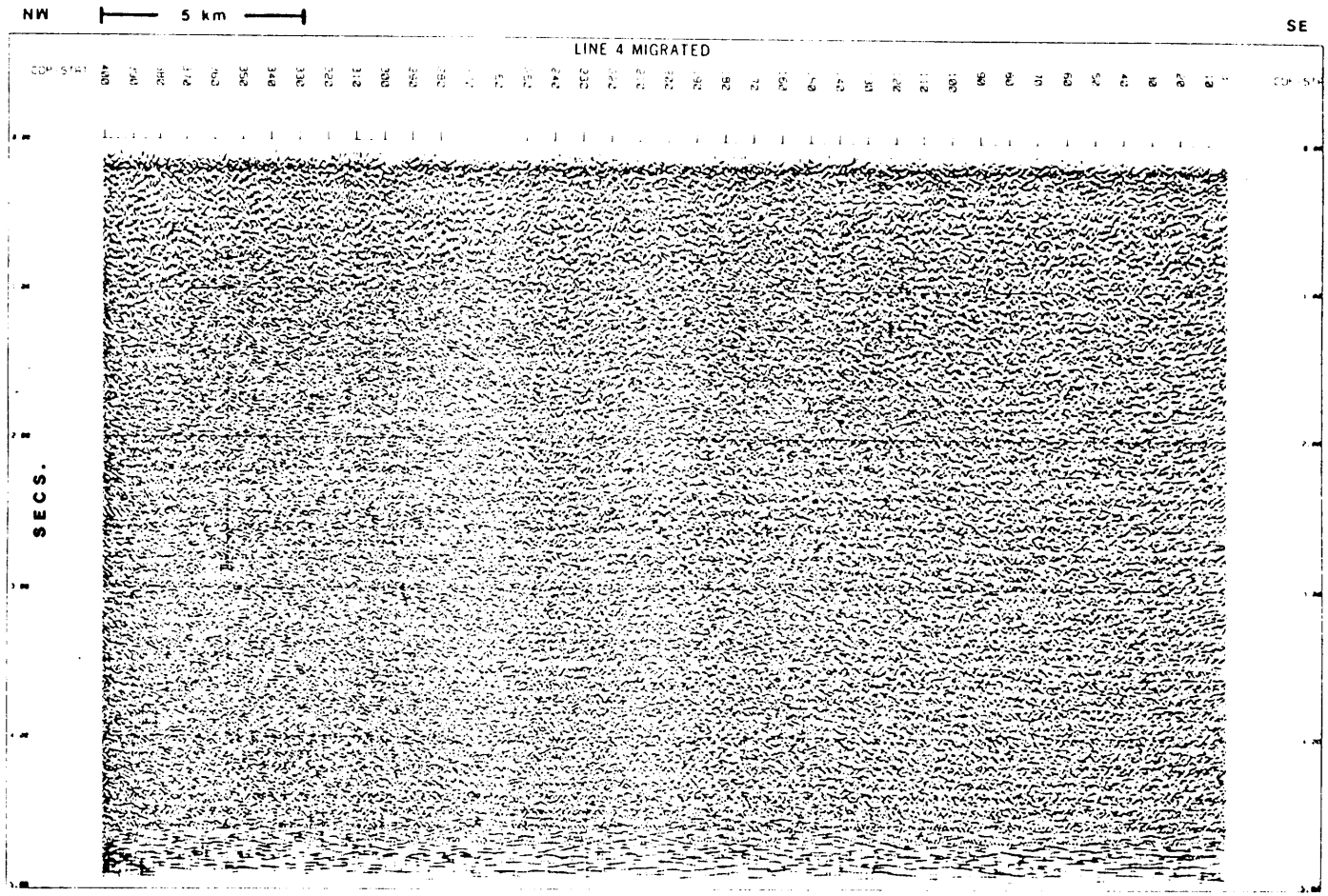
NW
5 km
SE
LINE 4 MIGRATED
SECS.

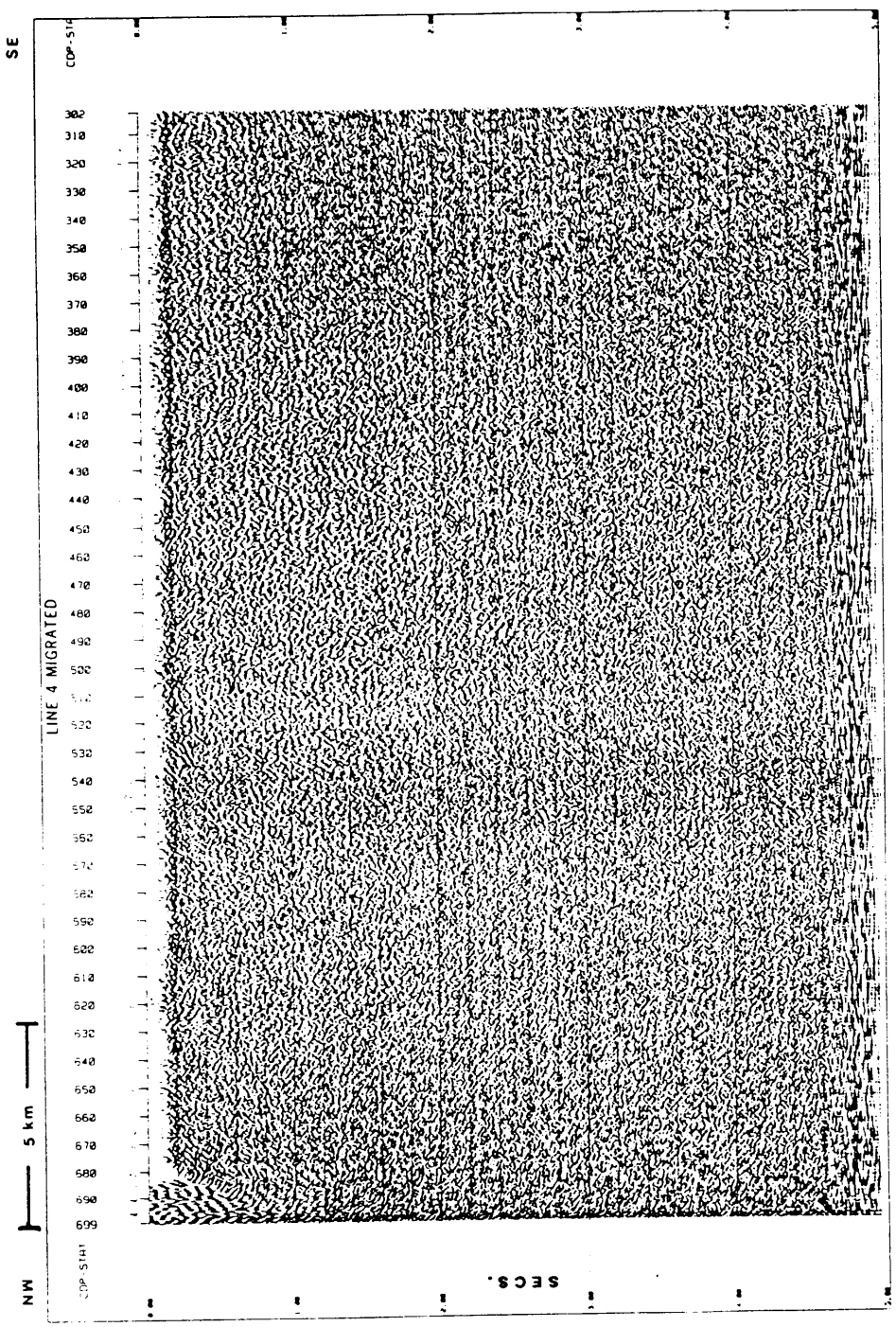
NW
SE
5 km
LINE 4 MIGRATED
SECS.
CDP-STH
CDP-STH
302
310
320
330
340
350
360
370
380
390
400
410
420
430
440
450
460
470
480
490
500
530
540
550
560
590
600
610
620
630
640
650
660
670
680
690
699

SE
NW
5 km
LINE 6
SECS.

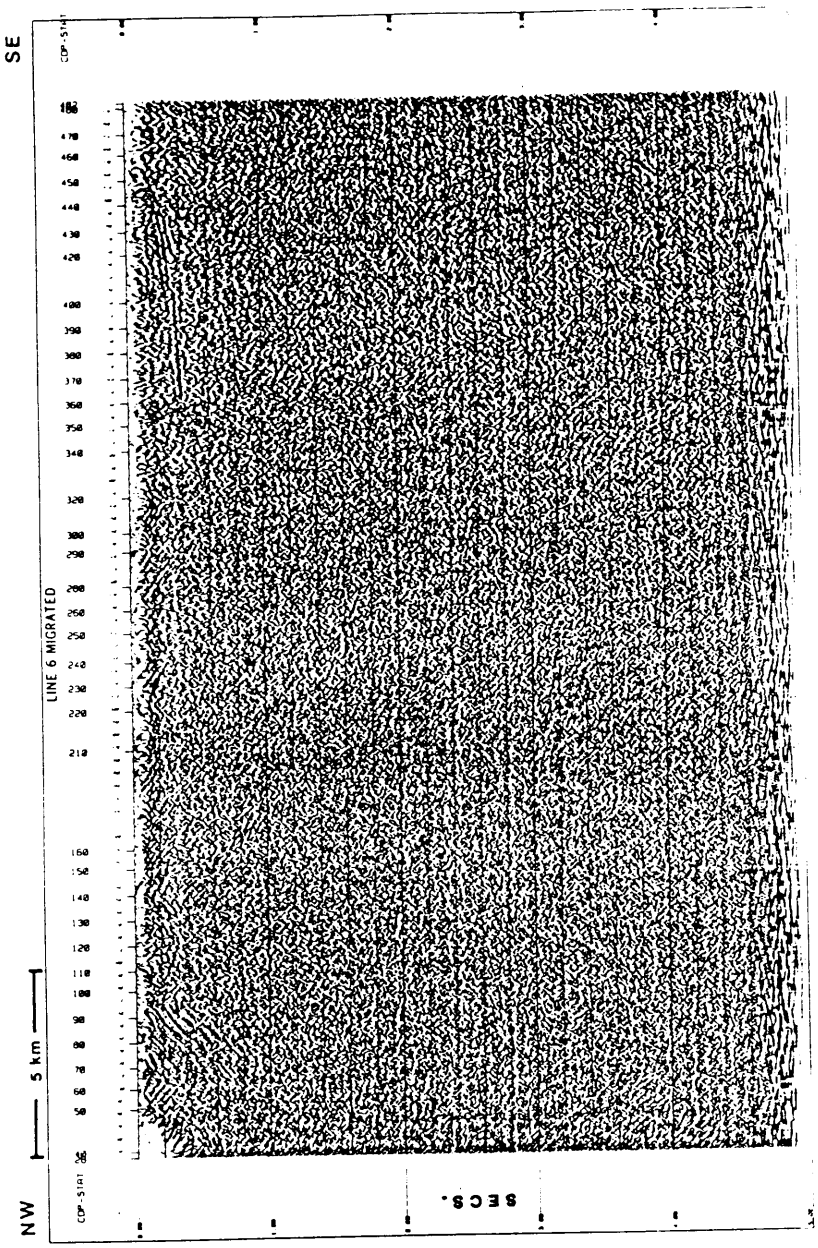
SE
NW
5 km
LINE 6 MIGRATED
SECS.

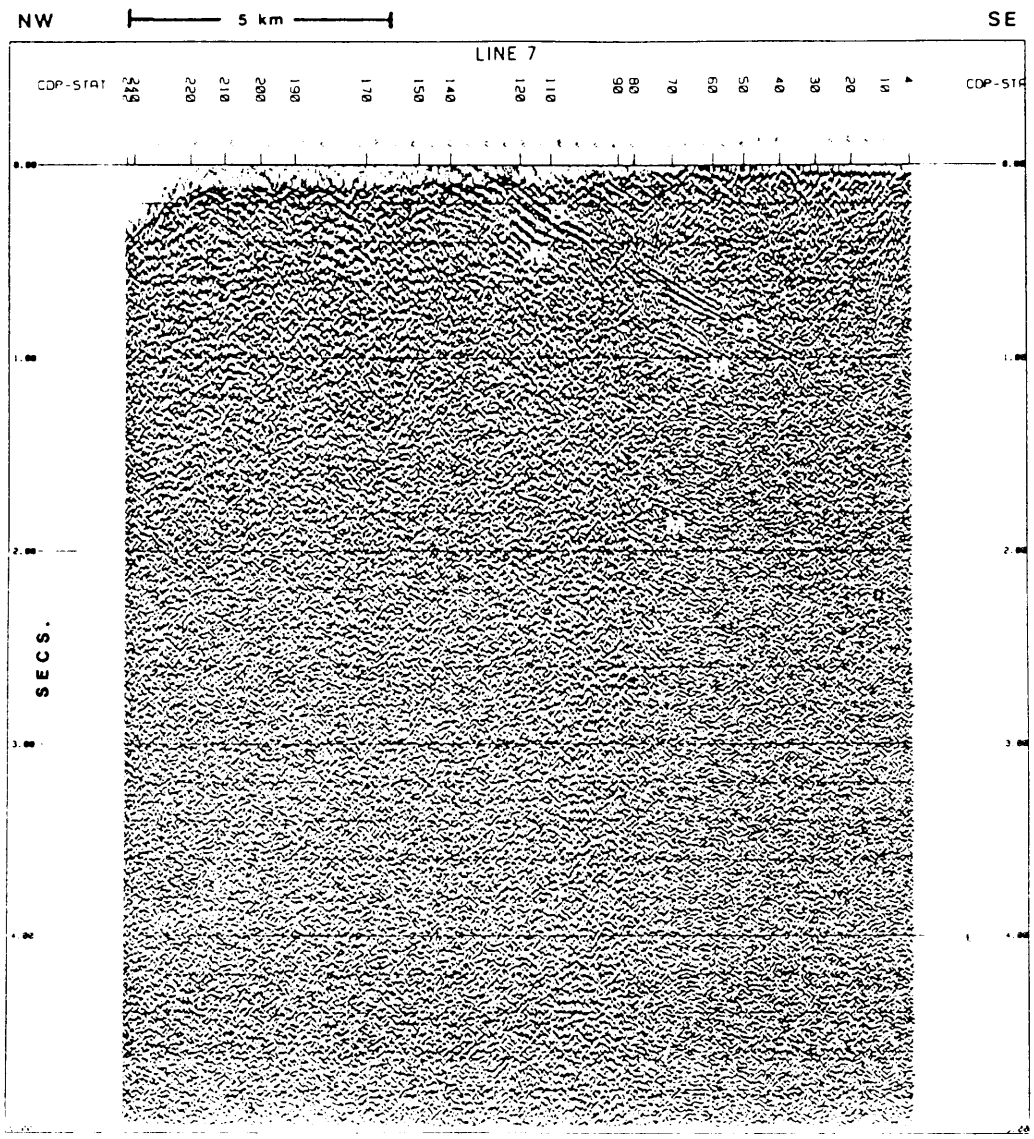
NW
5 km
SE
LINE 7
CDP-STAT
SECS.

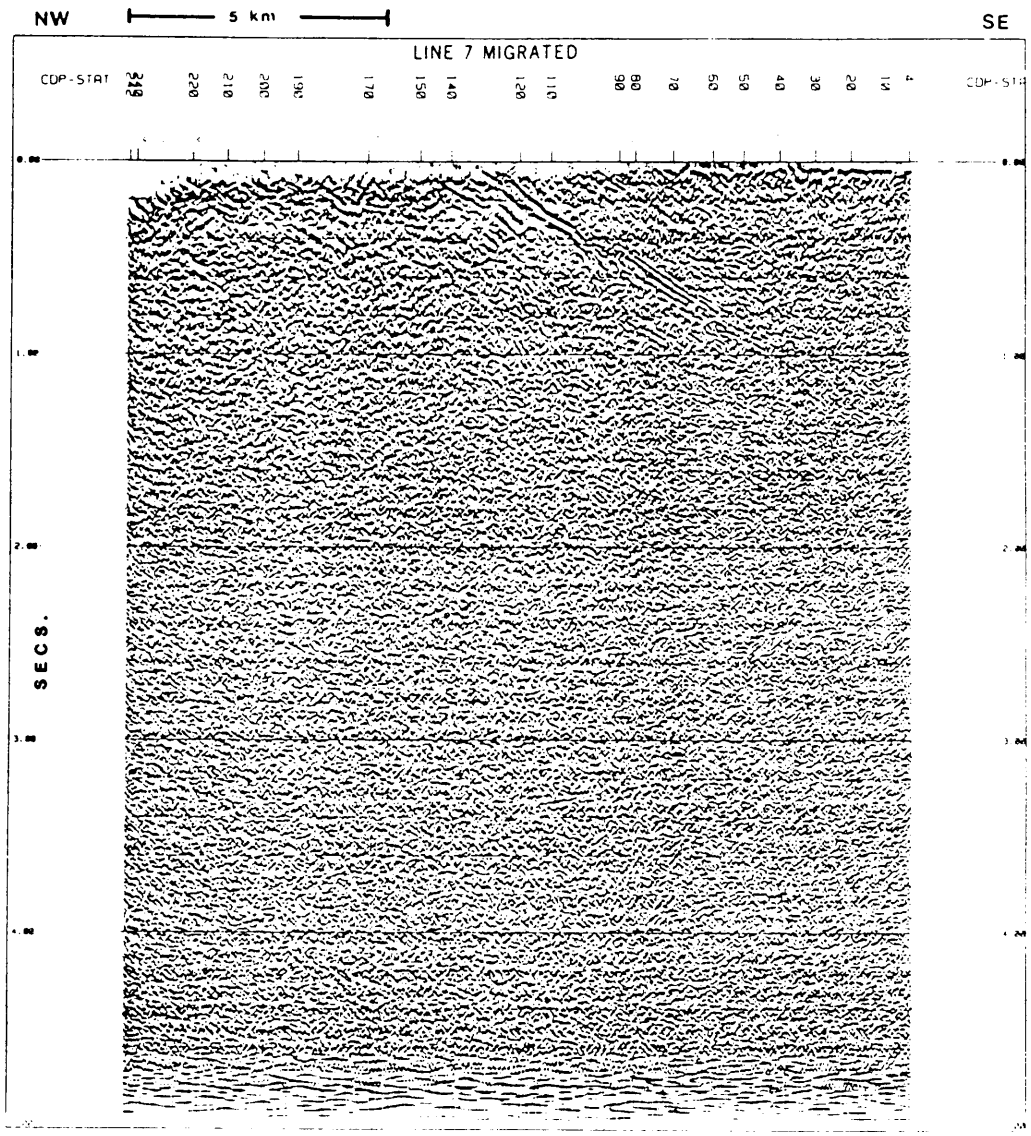
NW
5 km
SE
LINE 7 MIGRATED
CDP-STAT
SECS.

APPENDIX E.

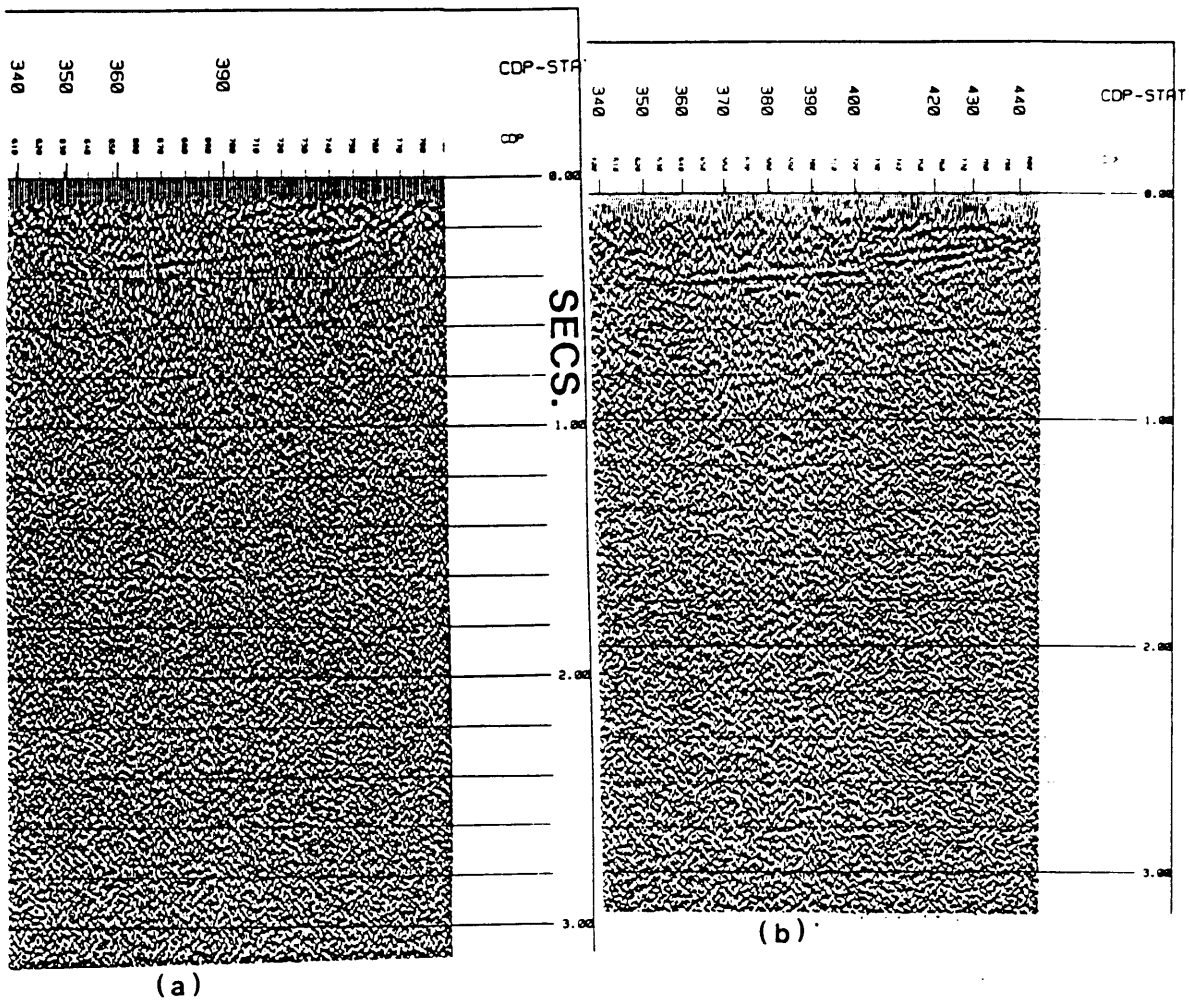

Effect of CDP line orientation on Line 6: Part of Line 6 containing the basin and a reflection from a basaltic intrusion (a) sorted with a straight CDP line perpendicular to the fault plane and (b) sorted with a modified-crooked CDP line. (Unmigrated and no vertical exaggeration)

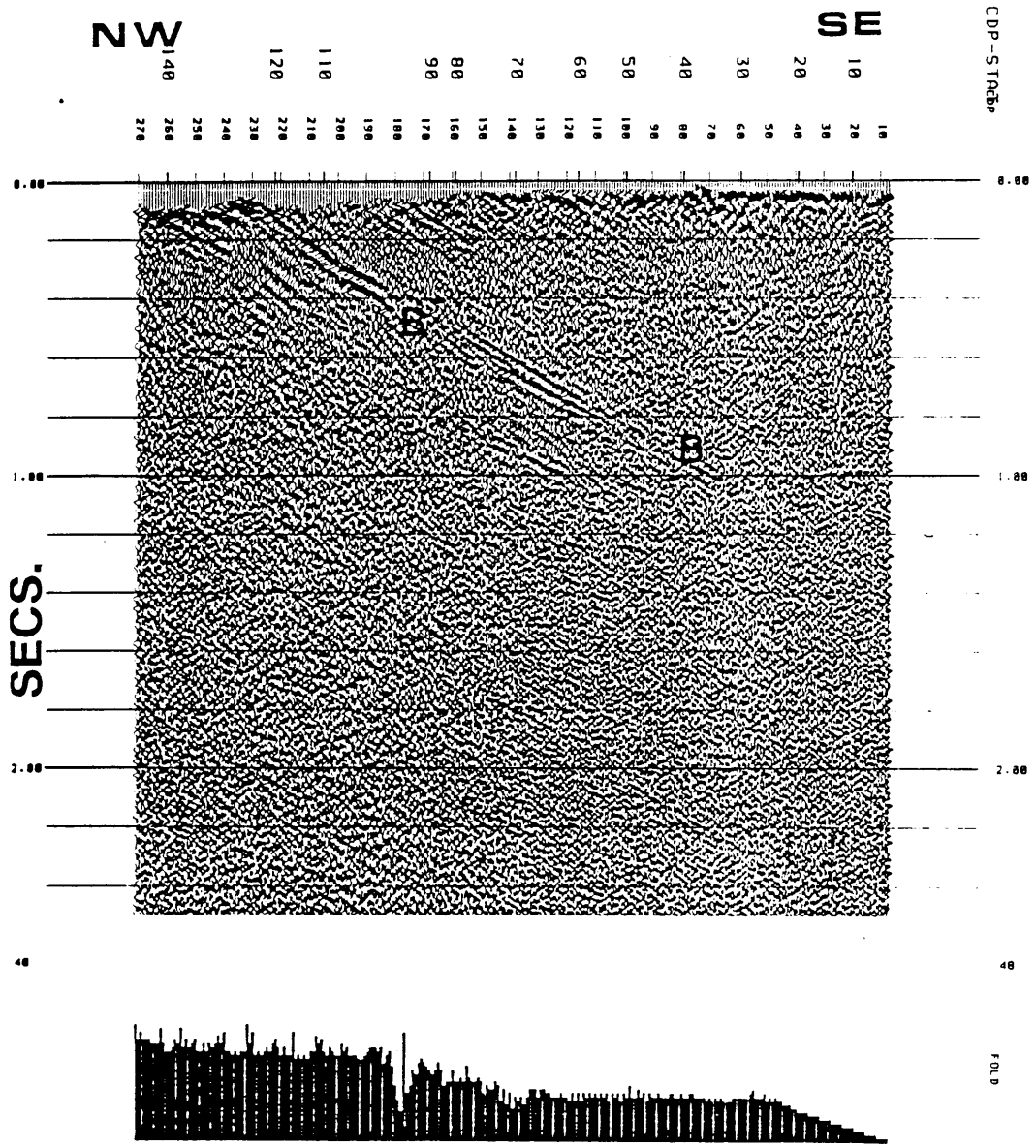

Effect of variations in CDP fold on data quality: Part of Line 7 after standard processing. Note that where the fold is 24 or greater the reflection from the fault (labeled 'B') is strong, but as the fold diminishes the reflection fades away. (Unmigrated and no vertical exaggeration)

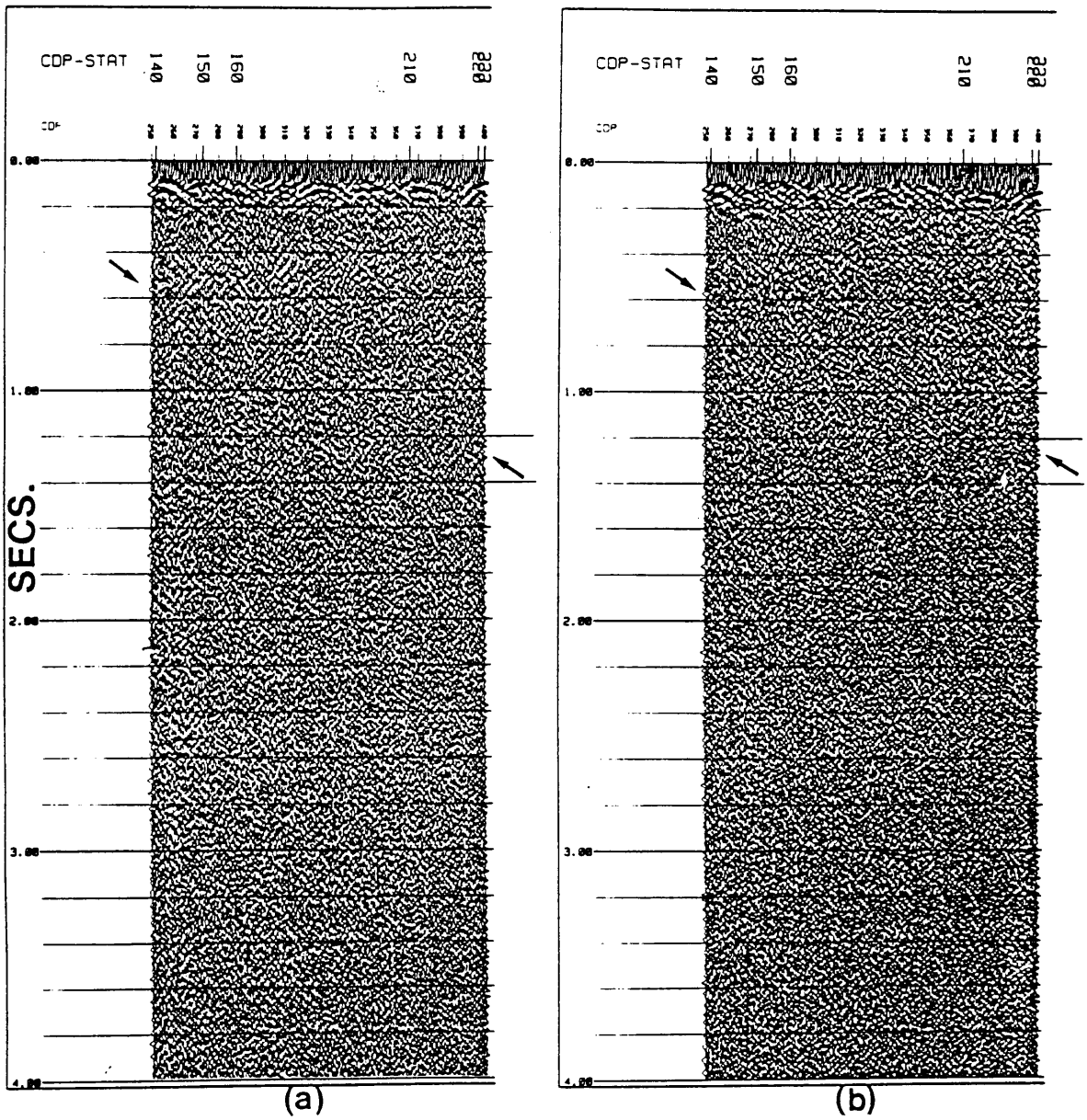

Part of Line 6 before (a) and after (b) application of residual statics corrections: Note the effect on the reflections marked by the arrows. (Unmigrated and no vertical exaggeration)

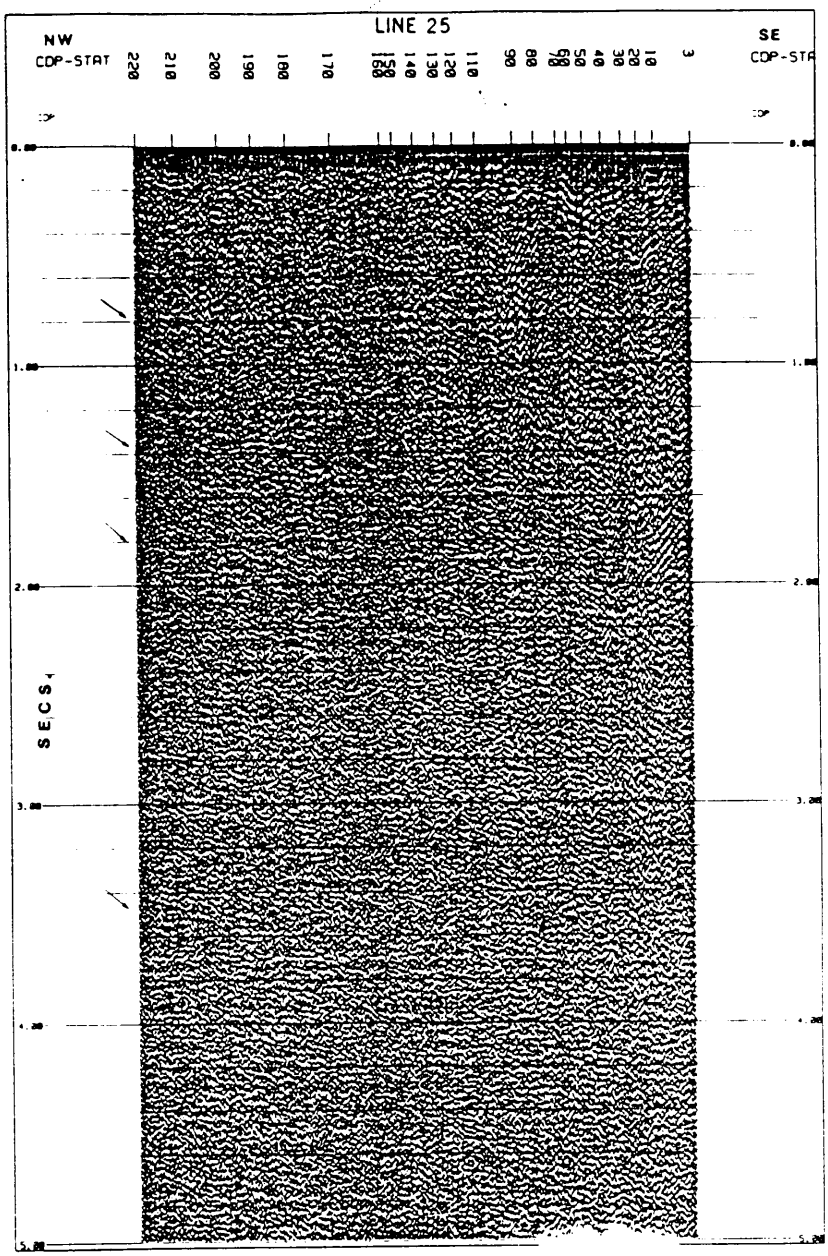

Line 25 with time-variant ARS: Enhanced reflections marked by arrows. (Unmigrated and no vertical exaggeration.)

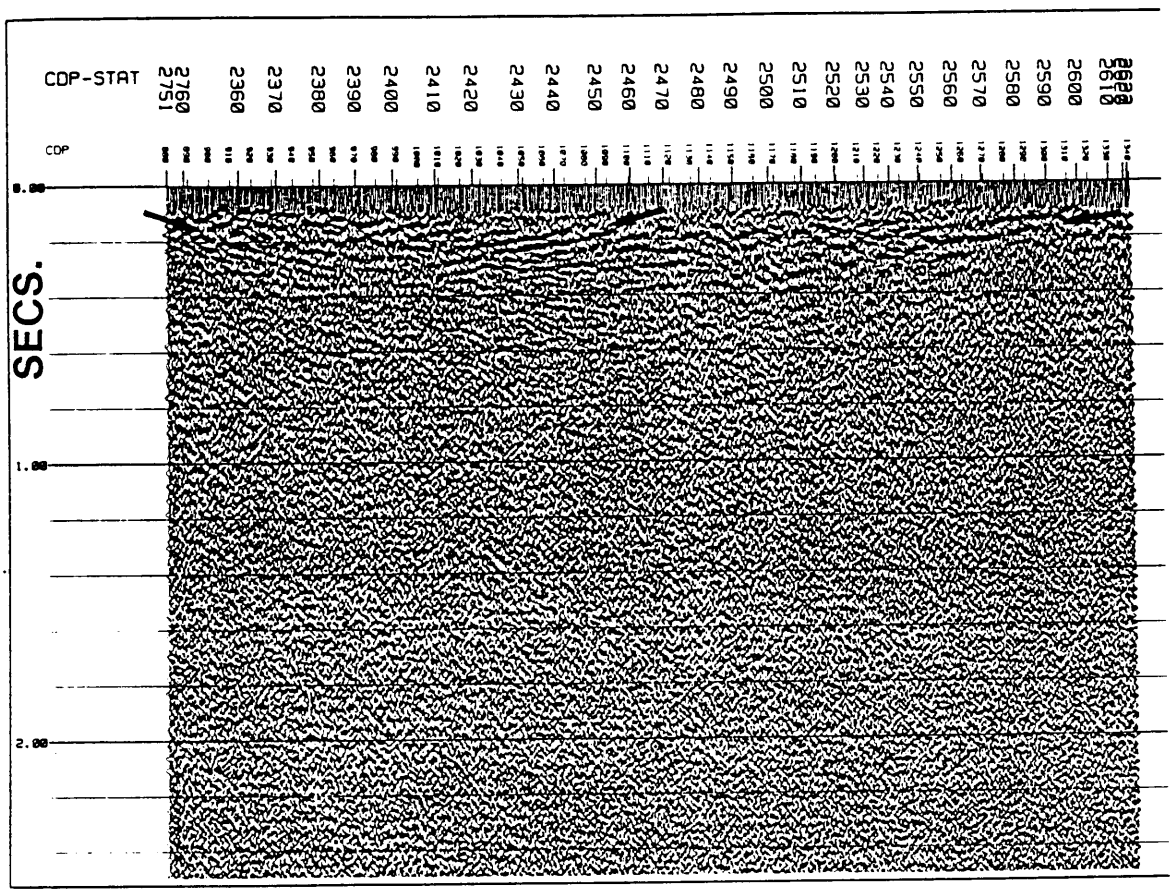

Part of Line 3 single-sweep section: Note the shallow reflections perhaps indicating a basin (marked by arrows). (Unmigrated)

The vita has been removed from the scanned document